Title 論文題目	Umbilical cord extracts improve osteoporotic abnormalities of bone marrow-derived mesenchymal stem cells and promote their therapeutic effects on ovariectomized rats （臍帯抽出物は骨粗鬆症に伴う骨髄間葉系幹細胞の異常性を改善し、卵巣摘出骨粗鬆症モデルラットに対する細胞治療の効果を改善する）
Author(s) 著　者	齋藤，憲
Degree number 学位記番号	甲第 2967 号
Degree name 学位の種別	博士（医学）
Issue Date 学位取得年月日	2017-03-31
Original Article 原著論文	札幌医学雑誌　第 86 巻 1 号（平成 30 年 3 月）
Doc URL	
DOI	
Resource Version	

Title

Umbilical cord extracts improve osteoporotic abnormalities of bone marrow-derived mesenchymal stem cells and promote their therapeutic effects on ovariectomized rats

Akira Saito[1], Kanna Nagaishi[2,3*], Kousuke Iba[1], Yuka Mizue[2,3], Takako Chikenji[2,3], Miho Otani[3], Masako Nakano[2], Toshihiko Yamashita[1], and Mineko Fujimiya[2,3]

1)Department of Orthopedic Surgery, Sapporo Medical University, Sapporo, Japan, 2) Second Department of Anatomy, Sapporo Medical University, Sapporo, Japan, 3) Department of Diabetic Cellular Therapeutics, Sapporo Medical University, Sapporo, Japan

*Corresponding author

Kanna Nagaishi

Second Department of Anatomy, Sapporo Medical University

S-1, W-17, Chuo-ku, Sapporo, Hokkaido 060-8556, Japan

Phone: +81-11-611-2111 (Ext.: 26470)

Fax: +81-11-618-4288

E-mail: kanna@sapmed.ac.jp

Abstract

Bone marrow-derived mesenchymal stem cells (BM-MSCs) are considered to be the most valuable source of autologous cell transplantation for tissue regeneration including osteoporosis. Although BM-MSCs are the primary cells to maintain the homeostasis of bone metabolism, their regenerative ability might be attenuated in postmenopausal osteoporosis patients. Therefore, we first demonstrated the abnormalities of BM-MSCs in an estrogen-deficient rat model constructed by ovariectomy (OVX-MSCs). Cell proliferation, osteogenic differentiation ability, and regulatory effects on osteoclasts were down-regulated in OVX-MSCs. The therapeutic effects of OVX-MSCs were decreased in OVX rats. Accordingly, we developed a new activator for BM-MSCs using human umbilical cord extracts, namely, Wharton's jelly extract supernatant (WJS) aiming to improve the functional abnormalities of OVX-MSCs. WJS improved cell proliferation and suppressive effects on activated osteoclasts in OVX-MSCs. Bone density, RANK expression and TRACP activity of osteoclasts were ameliorated by OVX-MSCs activated by WJS (OVX-MSCs-WJ) in OVX rats *in vivo*. Fusion and bone resorption activity of osteoclast were suppressed in RAW264.7 macrophage-induced osteoclasts via suppressing of *Nfatc1* by co-culturing with OVX-MSCs-WJ *in vitro*. In this study, we developed a new activator, WJS, which improved the functional

abnormalities and therapeutic effects of BM-MSCs on postmenopausal osteoporosis. (193)

Introduction

Postmenopausal osteoporosis, which is the most frequent form of osteoporosis, is caused by a reduction of estrogen secretion accompanying a decrease in ovarian function. Since estrogen maintains bone density by suppressing bone resorption[1,2], the number of patients with osteoporosis is increased in postmenopausal women, whose bone resorption activity is promoted along with the reduction of estrogen level. Approximately 50% of 65-year-old women have some experience of fractures due to postmenopausal osteoporosis at some point in their life[3]. Although hormone replacement therapy with estrogen is effective for postmenopausal osteoporosis, there is a risk of uterine cancer and breast cancer. Selective estrogen receptor modulators have been applied clinically instead of estrogen, but it is necessary to continue taking these for a long period of time. Therefore, a novel therapeutic method that balances bone formation and resorption is required urgently. Regenerative medicine using bone marrow-derived mesenchymal stem cells (BM-MSCs), which might have the ability to control both bone formation and resorption, has been focused on as an attractive method to meet these requirements.

MSCs are considered a highly useful cell source for regenerative medicine because of their multi-potentiality and high safety. MSCs have been focused on because of their variety of characteristics, such as strong capacity for self-renewal, pluripotency, reduced antigenicity, immunoregulatory functions, and ease of isolation and culture *in vitro* to obtain large numbers of cells for treatment[4]. Although MSCs can be obtained from various tissues, such as bone marrow, adipose tissue, umbilical cord (UC) blood and tissues[5], placenta[6], and dental pulp[7], BM-MSCs have been the most well explored, and efforts have been made for their clinical application due to their safety and efficacy in systemic administration[8]. Several clinical trials of cell therapies using BM-MSCs have already been reported in autoimmune diseases[9,10], chronic inflammatory disease[11,12], myocardial infarction[13], spinal cord injury[14], and osteoporosis[15].

Autologous transplantation of BM-MSCs has great benefits because of the low risk of rejection and exogenous infection and securing a stable cell source of MSCs. However, several functional abnormalities of BM-MSCs have been reported in osteoporosis patients[16,17,18]. Zhao and others reported abnormalities related to the differentiation of BM-MSCs. Estrogen potentially regulates the osteoblastic differentiation of human BM-MSCs via PI3K signaling or up-regulation of estrogen receptor alpha (ERα), which results in the diminished production of osteoblasts and excessive differentiation of adipocytes from BM-MSCs in postmenopausal osteoporosis patients. Turgeman et al. reported that BM-MSCs obtained from osteoporosis mice showed decreased cell proliferation and increased apoptosis *in vitro*[19]. Li and others reported that BM-MSCs derived from osteoporosis rats had clearly decreased proliferation ability and pluripotency-related gene expression compared to those derived from normal rats[20,21]. These reports suggest that BM-MSCs derived from patients with osteoporosis are not appropriate for cell therapy because of their abnormal functionality. However, the therapeutic effect of abnormal BM-MSCs for osteoporosis *in vivo* has yet to be clarified. Therefore, we first aimed to clarify the abnormalities of BM-MSCs derived from an estrogen-deficient osteoporosis model *in vitro* and investigated whether abnormal osteoporosis BM-MSCs exhibit sufficient therapeutic effects on osteoporosis *in vivo*.

To carry out autologous transplantation with abnormal BM-MSCs, these cells need to be remade into functional cells that might have therapeutic effects on abnormal bone metabolism. In this study, we focused on a novel activator, human UC extracts, which we named “Wharton’s jelly extract supernatant” (WJS). The UC is composed of embryonic tissues, including umbilical vessels, Wharton’s jelly (WJ), and amniotic membranes. These tissues are the source of fetal appendage-derived MSCs, which reportedly show high proliferative potential[22]. WJ and perivascular tissues contain a variety of growth factors, cytokines, extracellular matrix (ECM), and micro-vesicles, which may provide the necessary physiological environment to maintain the properties of fetal appendage-derived MSCs[23, 24]. An et al. reported that human UC blood-derived MSCs ameliorated bone mineral density in nude mice with ovariectomy (OVX)[25]. Therefore, we hypothesized that these biological components might activate abnormal BM-MSCs. The usefulness of WJ extracts has been reported as a coating agent for cell culture materials, which inhibited cellular senescence due to culture stress and enhanced cell proliferation of normal MSCs[26]. However, it has not been clarified whether WJS is useful for the functional improvement of abnormal BM-MSCs derived from an osteoporosis model. Thus, we next aimed to investigate the efficacy of WJS to improve abnormal BM-MSCs derived from an OVX osteoporosis rat model *in vitro*. Then, we investigated the therapeutic effects of activated BM-MSCs on the OVX model *in vivo*.

We investigated the activating effects of the novel cell activator WJS *in vitro* and the therapeutic effect of activated BM-MSCs *in vivo*. This method may allow autologous cell transplantation using a patient's own BM-MSCs not only for osteoporosis patients but also for other diseases in which autologous BM-MSCs are abnormal.

Results

Bone mineral density and histological findings of bone were abnormal in OVX rats

An osteoporosis model was constructed using rats by OVX and analyzed at 4, 8, and 12 weeks after surgery (Fig. 1a). In micro-computed tomography (CT) findings, the number and density of trabeculae were obviously reduced in the proximal tibia of OVX rats compared to Sham rats (Fig. 1b). Trabecular bone mass was reduced markedly depending on the period after OVX. In quantitative analysis of micro-CT images, bone volume fraction and trabecular number were significantly decreased and trabecular separation was significantly increased in OVX rats at 4 weeks after OVX ($P = 0.008$, Fig. 1c; $P < 0.015$, Fig. 1e; and $P < 0.0135$, Fig. 1f). Trabecular thickness was lower in OVX rats than in Sham rats at 12 weeks after OVX ($P = 0.021$, Fig. 1d). Histological findings of hematoxylin and eosin (H&E) staining in the proximal tibia at 12 weeks after OVX showed thinning and narrowing of the trabecular bone, which was similar to the findings observed in micro-CT (Fig. 1g). The expression levels of receptor activator of nuclear factor κ-B (RANK) in osteoclasts was increased in OVX rats (Fig. 1h). The number of tartrate-resistant acid phosphatase (TRACP)-positive osteoclasts was increased in OVX rats (Fig. 1i). The size of each osteoclast was larger in OVX rats than in Sham rats, which was determined by the intensity and area of TRACP expression. Serum TRACP levels were also significantly higher in OVX rats (n = 5) than in Sham rats (n = 5) at 12 weeks after OVX (P = 0.013, Fig. 1j).

Morphology and proliferative ability are abnormal in BM-MSCs derived from OVX rats

The morphological findings of BM-MSCs isolated from OVX rats (OVX-MSCs) were abnormal in phase contrast observations, with short and dull cell protrusions, enlarged cell area, flat shape, and disordered orientation of cells compared with BM-MSCs isolated from Sham rats (Sham-MSCs) (Fig. 2a). These findings were similarly observed from passage 0 (P0) to P2. The immunophenotype of cell surface antigens was similar between OVX-MSCs and Sham-MSCs (Fig. 2b). The proliferation of OVX-MSCs was significantly reduced compared with Sham-MSCs as follows. The cell growth of OVX-MSCs evaluated by population doubling time (PDT) at P2 was significantly increased compared to Sham-MSCs (P = 0.0071, Fig. 2c). Cell growth of OVX-MSCs as indicated by an MTT proliferation assay was significantly decreased compared to Sham-MSCs (P = 0.014 at 24 h, P = 0.012 at 48 h, and P = 0.01 at 72 h, Fig. 2d).

Expression of osteogenic differentiation factor and osteoclast regulating factor are abnormal in OVX-MSCs

The relative mRNA expression of Runt-related transcription factor 2 (*Runx2*), osteocalcin (*Ocn*), and estrogen receptor α (*Erα*), which are osteogenic differentiation factors, and osteoprotegerin (*Opg*), which is an osteoclast regulating factor, were downregulated in OVX-MSCs compared with Sham-MSCs (Fig. 2e).

Potential to differentiate into multiple mesenchymal lineages is altered in OVX-MSCs

Osteogenic differentiation ability was decreased in OVX-MSCs compared with Sham-MSCs as shown by the decrease of alkaline phosphatase-positive cells (Fig. 2h, upper panels). Conversely, adipogenic differentiation ability was enhanced in OVX-MSCs compared with Sham-MSCs as shown by the increase of Oil red O-positive lipid droplets in the cytoplasm of BM-MSCs (Fig. 2h, lower panels).

OVX-MSCs do not ameliorate osteoporosis in OVX rats

The experiment was carried out as shown in Fig. 3a. OVX rats were treated with Vehicle (OVX-Vehicle rats), Sham-MSCs (OVX-Sham-MSCs rats), or OVX-MSCs (OVX-OVX-MSCs rats). Bone tissues of the rats were evaluated at 8 weeks after the administration of each type of BM-MSCs. In micro-CT analysis, Sham-MSCs inhibited the progression of osteoporosis, as indicated by the increase of trabecular bone volume, trabecular thickness, trabecular number, and decrease of trabecular separation in the proximal tibia of OVX rats compared with OVX-Vehicle rats (P = 0.008, Fig. 3c; P = 0.029, Fig. 3d; P = 0.013, Fig. 3e; P = 0.017, Fig. 3f). PKH26-labeled Sham-MSCs were distributed in the bone marrow of OVX rats at 24 h after cell administration. The number of distributed cells was decreased at day 3 and quickly disappeared in a few days (see Supplementary Fig. S1). Conversely, OVX-MSCs did not show adequate therapeutic effects in OVX rats, that is, there was no significant change of these indicators in OVX rats compared with OVX-Vehicle rats (P = 0.197, Fig. 3c; P = 0.212, Fig. 3d; P = 0.299, Fig. 3e; P = 0.246, Fig. 3f).

Histological findings of tibia bone from OVX rats showed similar changes as observed in micro-CT. Thinning and narrowing of the trabecular bone and fat deposits in the bone marrow cavity were observed in OVX-Vehicle rats compared with OVX-Sham-MSCs rats with H&E staining (Fig. 3g, left panels). The administration of Sham-MSCs improved these histological changes in the tibia of OVX rats (Fig. 3g, middle panels), while OVX-MSCs did not improve the histological damage (Fig. 3g, right panels). The expression levels of RANK were decreased in OVX-Sham-MSCs rats compared with OVX-Vehicle rats, while these were not changed in OVX-OVX-MSCs rats compared with OVX-Vehicle rats (Fig. 3h). The number of TRACP-positive osteoclasts and expression levels of TRACP were decreased in the tibia of OVX-Sham-MSCs rats compared with OVX-Vehicle rats. The size of each osteoclast was smaller in OVX-Sham-MSCs rats than in OVX-Vehicle rats. Conversely, OVX-MSCs did not suppress the size of osteoclasts or expression levels of TRACP in the osteoclasts of OVX-OVX-MSCs rats compared with OVX-Sham-MSCs rats (Fig. 3i). Serum TRACP levels were significantly lower in OVX-Sham-MSCs rats (n = 5) than in OVX-Vehicle rats (n = 5) and OVX-OVX-MSCs rats (n = 5) at 8 weeks after the administration of each type of BM-MSCs (P = 0.006 vs. OVX-Vehicle rats, P = 0.037 vs. OVX-OVX-MSCs rats, Fig. 3j).

WJS improves the morphology and proliferative ability of OVX-MSCs

WJS were to confirm that the remaining cellular components have lost their viability by incubating at 37°C in 5% CO_2 with 10% of FBS for 96 hours. Then, OVX-MSCs were cultured with an appropriate concentration of WJS for 48 h. In phase contrast observations, OVX-MSCs cultured with WJS (OVX-MSCs-WJ[+]) changed by having thinner and longer cell protrusions, reduced cell area, and spindle-shaped and well orientated cells (Fig. 4a). The immunophenotype of cell surface antigens did not change in OVX-MSCs-WJ(+) compared with OVX-MSCs cultured without WJS (OVX-MSCs-WJ[-]) (Fig 4b). The proliferative ability of OVX-MSCs-WJ(+) was improved significantly as indicated by PDT and MTT proliferative assays compared with OVX-MSCs-WJ(-) (P = 0.036, Fig. 4c; P = 0.025 at 24 h, P = 0.011 at 48 h, Fig. 4d).

WJS partially alters osteogenic differentiation factors but not osteoclast regulating factor in OVX-MSCs

The relative mRNA expression of *Ocn* were rather downregulated, while *Runx2*, *Erα*, and *Opg* were not changed in OVX-MSCs-WJ(+) compared with OVX-MSCs-WJ(-) (Fig. 4e).

WJS suppresses differentiation osteogenic but not alters adipogenic differentiation in OVX-MSCs

Osteogenic differentiation were rather suppressed in OVX-MSCs-WJ(+) compared with OVX-MSCs-WJ(-) as shown by the decrease in alkaline phosphatase-positive cells (Fig. 4h, upper panels). Conversely, adipogenic differentiation ability was not changed in OVX-MSCs-WJ(+) compared with OVX-MSCs as shown by the number of Oil red O-positive lipid droplets in the cytoplasm of BM-MSCs (Fig. 4h, lower panels).

OVX-MSCs-WJ(+) ameliorate osteoporosis in OVX rats

This experiment was carried out as shown in Fig. 5a. Bone tissues of rats were evaluated at 8 weeks after the administration of each type of BM-MSCs. In micro-CT analysis of the proximal tibia, OVX-MSCs-WJ(+) inhibited the progression of osteoporosis, as indicated by the increase of trabecular bone volume and trabecular thickness in OVX rats compared with OVX-Vehicle rats (Fig. 5b, $P = 0.049$; Fig. 5c, $P = 0.027$; Fig. 5d). Conversely, OVX-MSCs-WJ(-) did not show an adequate therapeutic effect in OVX rats, that is, there was no significant change of these indicators in OVX rats compared with OVX-Vehicle rats (Fig. 5b, $P = 0.157$; Fig. 5c, $P = 0.124$; Fig. 5d, $P = 0.194$; Fig. 5e, $P = 0.372$; Fig. 5f).

Histological findings of the tibia in OVX rats showed similar changes as observed in micro-CT. Thinning and narrowing of the trabecular bone and fat deposits in the bone marrow cavity were observed in OVX-Vehicle rats with H&E staining (Fig. 5g, left panels). While the administration of OVX-MSCs-WJ(+) improved these histological changes (Fig. 5g, right panels), OVX-MSCs-WJ(-) did not improve the histological damage (Fig. 5g, middle panels). The expression levels of RANK were decreased in OVX-MSCs-WJ(+) rats compared with OVX-Vehicle rats, while these were not changed in OVX-MSCs-WJ(+) rats compared with OVX-Vehicle rats (Fig. 5h). The number of TRACP-positive osteoclasts and expression levels of TRACP were decreased in OVX-MSCs-WJ(+) rats compared with OVX-Vehicle rats. The size of each osteoclast was smaller in OVX-MSCs-WJ(+) rats than in OVX-Vehicle rats. Conversely, the administration of OVX-MSCs-WJ(-) did not suppress the size of osteoclasts or expression levels of TRACP compared with OVX-MSCs-WJ(+) (Fig. 5h). Serum TRACP levels were significantly lower in OVX-MSCs-WJ(+) rats (n = 5) than in OVX-Vehicle rats (n = 5) and OVX-MSCs-WJ(-) rats (n = 5) at 8 weeks after administration of each type of BM-MSCs (P = 0.001 vs. OVX-Vehicle, P = 0.005 vs. OVX-MSCs-WJ(-), Fig. 5i).

Sham-MSCs and OVX-MSCs-WJ(+) ameliorate maturation and excessive activation of macrophage-derived osteoclasts

Systemic administration of Sham-MSCs and OVX-MSCs-WJ(+) apparently improved bone mineral density *in vivo*. Since the number and activity of osteoclasts in bone tissue were suppressed by these therapies, we investigated whether osteoclast activity was regulated by BM-MSCs as the mechanism of MSC therapy. The macrophage cell line RAW264.7 was differentiated into macrophage-derived osteoclasts by the addition of receptor activator of nuclear factor κ-B ligand (RANKL) alone or the combination of RANKL and the MEK inhibitor PD98059 *in vitro* (Fig. 6a). Macrophages were fused into multinucleated osteoclasts (Fig. 6b) and TRACP activity in the culture supernatant of macrophage-derived osteoclasts was increased at 72 h after induction with RANKL ($P < 0.05$; Fig. 6c). Morphologically, osteoclasts became larger and more matured by the addition of RANKL and PD98059 in combination rather than RANKL alone (Fig. 6b). TRACP activity in the culture supernatant of osteoclasts was also further increased by their combination ($P < 0.05$, Fig. 6c). Next, mature macrophage-derived osteoclasts and each type of BM-MSCs were co-cultured indirectly for 24 h (Fig. 6d). Expansion of the size of osteoclasts was suppressed by co-culturing Sham-MSCs and OVX-MSCs-WJ(+) compared with Vehicle and OVX-MSCs-WJ(-) (Fig. 6e). TRACP activity in the culture supernatant was significantly suppressed by co-culturing Sham-MSCs and OVX-MSCs-WJ(+) compared with Vehicle ($P < 0.05$, Fig. 6f). The inhibitory effect on TRACP activity by OVX-MSCs-WJ(-) was lower than that of Sham-MSCs and OVX-MSCs-WJ(+).

Sham-MSCs and OVX-MSCs-WJ(+) improve the excessive expression of osteoclast differentiation factors, fusion promoting factor, and activating factors in macrophage-derived osteoclasts

The relative mRNA expression levels of various factors that promote the differentiation (e.g., *c-fms*), formation (e.g., *Dc-stamp*), and activity (e.g., *Nfatc1*, *Cathepsin-k*, *Clcn7*, and *Atp6i*) of osteoclasts were significantly suppressed by OVX-MSCs-WJ(+), similar to Sham-MSCs ($P < 0.05$; Fig. 6g), while they were not repressed by OVX-MSCs.

Discussion

Since BM-MSCs derived from an OVX osteoporosis rat model had reduced therapeutic efficacy, we created a new activation method for BM-MSCs to improve their therapeutic effects in autologous transplantation. We focused on the UC extract (i.e., WJS), and demonstrated its value to improve the abnormalities of BM-MSCs due to estrogen deficiency. This is the first study to investigate the significant potential of WJS to ameliorate abnormal BM-MSCs caused by osteoporosis. BM-MSCs activated by WJS had improved proliferative ability and regulatory effects on the excessive osteolytic properties of osteoclasts, which improved histological damage to bone and facilitated the recovery of trabecular bone density in micro-CT analysis.

BM-MSCs isolated from OVX rats (OVX-MSCs) had morphological abnormalities. Cell area was expanded irregularly and flattened with an increase of cytosolic actin filaments in OVX-MSCs, while Sham-MSCs maintained their spindle shape, were slim, and had a uniform cell size. Cell size in BM-MSCs reportedly correlates with the stemness, proliferation and differentiation ability, and tissue regenerative capacity of stem cells[27]. According to this, the abnormalities in the size and shape of OVX-MSCs predicted the following functional disorders of these cells.

Cell proliferation in OVX-MSCs was significantly decreased. The osteogenic and adipogenic differentiation abilities of OVX-MSCs were abnormal. These were correlated with a decrease of alkaline phosphatase expression or increase of lipid droplet expression in OVX-MSCs, respectively. In OVX-MSCs, the expression of *Runx2*, *Ocn*, and *ER*α was downregulated. Furthermore, OVX-MSCs could not regulate excessively activated osteoclasts with high osteolytic capacity, which was indicated by the lower mRNA expression of *Opg*. Runx2, which is an essential transcription factor for osteoblast differentiation and osteogenesis[28], Ocn, which is involved in solid bone formation due to calcification of the ECM[29] is essential for osteogenesis in BM-MSCs.

ERα is also important for the formation of cortical bone via intracellular Wnt-β-catenin signaling in osteoprogenitor cells, which were differentiated from BM-MSCs[30]. Conversely, OPG binds to RANK strongly as a decoy receptor of RANKL, which is a trigger for osteoclast differentiation, and subsequently suppresses the activity of the essential transcription factor NFATc1[31]. Since OVX-MSCs had various and complex abnormalities, such as inappropriate differentiation potential and decrease of their regulatory capability for osteoclasts, it was speculated that these abnormalities might contribute not only to the reduction of bone density but also to the loss of their therapeutic effects in OVX rats.

As expected, OVX-MSCs had reduced therapeutic effects in OVX rats. Bone strength decreases in osteoporosis, which is indicated by bone volume fraction and bone quality. Bone strength and its microstructure have been evaluated by micro-CT in the OVX model[32]. Bone quality have been indicated by trabecular thickness, number, and separation in microstructure. In this study, OVX-MSCs did not improve all of these indicators, while Sham-MSCs improved them sufficiently, indicating that OVX-MSCs could not achieve therapeutic effects for both strength and bone microstructure. This was consistent with the histological findings of the absence of an improvement of trabecular bone and the presence of fat deposits in the bone marrow cavity. Furthermore, serum TRACP levels and the expression of RANK and TRACP in osteoclasts localized at the proximal end of the tibia were not decreased sufficiently in OVX rats treated with OVX-MSCs compared with Sham-MSCs *in vivo*. The reduction of the therapeutic effects of OVX-MSCs was considered by the accumulation of functional abnormalities in these cells, as shown *in vitro*.

We developed UC extracts, namely WJS, as an activator of OVX-MSCs to improve their abnormalities. The morphological and functional abnormalities of OVX-MSCs were improved by WJS. Expansion of cell area, flattening, and irregularities of the size and shape of the cells were improved. The proliferation of OVX-MSCs was increased by the addition of WJS, as indicated by the reduction of PDT and enhancement of the uptake of water-soluble tetrazolium salt (WST)-8 in the MTT proliferation assay. An improvement of cell proliferation is thought to be beneficial in cell therapy to secure an adequate number of cells from bone marrow within a short period of time. Interestingly, WJS rather suppressed the osteogenic differentiation of OVX-MSCs, which were indicated by low alkaline phosphatase expression in OVX-MSCs activated with WJS. These were also indicated by the alteration of the mRNA expression of osteogenic differentiation factors, *Ocn*. Ulrich reported that osteogenic differentiation potential was low in placenta-derived MSCs which were correlated with the expressions of both Runx2 and Twist2[33]. Twist2 inhibits the expression of Runx2 downstream targets, thus blocking the osteogenesis by interacting with Runx2[34]. Since OVX-MSCs treated with WJS might reveal similar characteristics as UC-MSCs, we thought that osteogenic differentiation was decreased in OVX-MSCs-WJ as similar as UC-MSCs or placenta-derived MSCs. Conversely, WJS did not alter *Opg* expression in OVX-MSCs, which suggested the presence of another factor derived from OVX-MSCs-WJ(+) to regulate osteoclast activity instead of OPG.

Since UC consists of amnion, blood vessels, and interstitial components including UC-MSCs and WJ, WJS contains various physiologically active substances, such as growth factors, ECM, amino acids, exosomes, and nucleic acids represented by miRNAs, which originate in these tissue components[35-37]. The cellular components of UC represented by UC-MSCs produce large amounts of autocrine/paracrine factors, such as insulin-like growth factor I (IGF-I), basic fibroblast growth factor (b-FGF), transforming growth factor β, platelet-derived growth factor (PDGF), epidermal growth factor (EGF), hyaluronic acid, collagen, glycosaminoglycans, and miRNAs[23,35]. Preconditioning BM-MSCs with IGF-1 and b-FGF in combination induces the expression of cell survival-related factors, such as IGF-1, FGF-2, Akt, GATA-4, and Nkx 2.5, and downregulates cell senescence- and apoptosis-related factors, such as p16(INK4a), p66, p53, Bax, and Bak in BM-MSCs[38,39]. PDGF and b-FGF are essential components for the growth-promoting effects of BM-MSCs[40]. EGF induces growth factor production and the paracrine activity of MSCs via EGF-EGF receptor 1 signaling, including a mitogen-activated protein kinase-extracellular-signal-regulated kinase-dependent manner[41]. Recent reports identified critical roles of various microRNAs (miR) as regulators of MSCs via modifying gene expression either by inhibiting translation or by stimulating the degradation of target mRNAs. Minayi et al. reported that MiR-210 upregulates the proliferation of BM-MSCs[42]. Lv et al. reported that MiR-21 suppresses the apoptosis of BM-MSCs via activation of PI3K/Akt pathway[43]. MiR-148a and miR-148b, which are found in umbilical cord blood MSCs-derived exosomes, reportedly regulate the proliferation of umbilical cord blood MSCs by upregulating NF-κB or hedgehog signaling[44]. Considering these reports, WJS might have improved the proliferation of OVX-MSCs strongly as it contains a cocktail of cell activation factors.

In vivo treatment with WJS-activated OVX-MSCs significantly improved trabecular bone volume, trabecular thickness, and number and separation of tibia in OVX rats, as observed with micro-CT. These improvements were consistent with the recovery of histological finding of bone tissues and the reduction of RANK expression. RANK is the receptor on osteoclast precursor cells, which transmits intracellular signals essential for differentiation and activation of osteoclasts by binding with RANK ligand (RANKL), while OPG is a soluble decoy receptor for RANKL to inhibit its action[45]. RANKL-RANK-OPG system is a major regulator to determine the bone resorption by osteoclasts. In postmenopausal osteoporosis, bone resorption is increased by the production of monocyte related cytokine, such as IL-1, IL-6 and TNF-α, which induces the expression of RANKL in bone tissues and enhances RANKL-RANK mediated osteoclastogenesis[46]. On the other hand, UC-MSCs has known to exhibit immunosuppressive effects for monocytes by regulating cytokine production[47]. Considering from the similar characteristics of OVX-MSCs-WJ(+) to UC-MSCs, WJS might change the function of OVX-MSCs to exert immunoregulatory effects for osteoclast by regulating RANK signaling. These findings were correlated with the decrease of TRACP-positive osteoclasts in the OVX-MSCs-WJ(+) group compared with the vehicle and OVX-MSCs-WJ(-) groups *in vivo*. Since the very small number of administered MSCs localized in the bone tissue, the therapeutic effect of MSCs might not depend on the direct osteogenic differentiation of MSCs itself.

To confirm the detailed regulatory effects of OVX-MSCs-WJ(+) on osteoclasts, we co-cultured OVX-MSCs-WJ(+) with osteoclasts *in vitro*. OVX-MSCs-WJ(+) suppressed the fusion and enlargement of macrophage derived osteoclasts. Expression of osteoclast activating factors and TRACP levels in the culture supernatants of osteoclasts were also suppressed by culturing with OVX-MSCs-WJ(+). Although *Opg* expression was lower in OVX-MSCs-WJ(+) than Sham-MSCs, the osteoclast regulating effect of OVX-MSCs-WJ(+) was similar to that of Sham-MSCs. Yang et al. reported that OPG secretion was increased rapidly during BM-MSCs differentiation into osteoblasts, which inhibited osteoclast formation and bone absorption via the suppression of binding of RANKL to RANK. In addition, the expression of monocyte related cytokines, which enhanced the activation of RANK signaling, might be suppressed by functional MSCs[47]. It is known that *c-fms* enhances the differentiation of progenitor cells to osteoclasts, *Nfatc1* is a master transcription factor of osteoclasts in the downstream of the RANK pathway, *Cathepsin-k* is a degradation factor of type 1 collagen, *Clcn7* is a chlorine transporter that promotes bone resorption, *Atp6i* is an acid transporter that promotes bone resorption, and *Dc-stamp* specifically promotes the fusion of macrophages and multinucleation of osteoclasts. All of these factors were significantly decreased in the osteoclasts which were cultured with OVX-MSCs-WJ(+) and Sham-MSCs. Considering from these, Sham-MSCs and OVX-MSCs-WJ(+) successfully regulated osteoclast activity and maturation appropriately via different or overlapping mechanism. Since this effect was observed in indirect co-culture of BM-

MSCs and osteoclasts, a paracrine effect of BM-MSCs might have contributed to this effect.

In conclusion, we developed a novel method to activate abnormal BM-MSCs derived from a postmenopausal osteoporosis rat model using human UC extracts (WJS), and demonstrated the morphological and functional improvement of OVX-MSCs *in vitro*. We also demonstrated that WJS enhanced the therapeutic effects of OVX-MSCs on OVX rats *in vivo*. The site of action of WJS on OVX-MSCs and their therapeutic mechanism for osteoporosis were shown in Fig. 7. This method may provide a great benefit for the autologous transplantation of BM-MSCs in patients with osteoporosis induced not only by postmenopause but also by other reasons.

Methods

Animal model of osteoporosis

Eight-week-old female Wistar rats weighing 135–145 g were purchased from Japan SLC, Inc. (Shizuoka, Japan). The rats were housed in a temperature-controlled room (21 ± 1 °C) with a 12 h light/dark cycle and given free access to food and water. The rats received either a sham operation (Sham) or OVX under general anesthesia. The sham operation was performed using the same surgical procedure as for OVX, but without removing the ovaries. Both Sham and OVX rats underwent minimal surgery through a dorsal approach[48]. All methods for the animal experiments were performed in accordance with the relevant guidelines and regulations of the Animal Experiment Committee of Sapporo Medical University (Sapporo, Japan). All experimental protocols and studies were approved by the Animal Experiment Committee of Sapporo Medical University (Sapporo, Japan).

Study design

At first, the rats were divided into 2 groups: (1) rats with sham operation (Sham rats; n = 5), (2) rats with OVX (OVX rats; n = 15). The rats were sacrificed at 4, 8, and 12 weeks after surgery. Next, the OVX rats were divided into 3 groups at 4 weeks after OVX: (1) OVX rats administered vehicle (OVX + Vehicle; n = 5), (2) OVX rats administered Sham-MSCs (OVX + Sham-MSCs; n = 5), and (3) OVX rats administered OVX-MSCs (OVX + OVX-MSCs; n = 5). The rats were sacrificed at 8 weeks after each administration. Furthermore, the rats were divided into 3 groups at 4 weeks after OVX: (1) OVX rats administered vehicle (OVX + Vehicle; n = 5), (2) OVX rats administered OVX-MSCs not activated with WJS (OVX + OVX-MSCs-WJ[-]; n = 5), and (3) OVX rats administered OVX-MSCs activated with WJ (OVX + OVX-MSCs-WJ[+]; n = 5). The rats were sacrificed at 8 weeks after each administration.

Evaluation of bone mass and microarchitecture by micro-CT

The right tibias from each rat was isolated and fixed in 4% ethanol for micro-CT. The tibias were scanned with a micro-CT system (ScanXmate-L090; Comscantecno, Yokohama, Japan) operated at a lamp voltage of 75 kV and current of 100 μA using the software X sys FP Version 1.7 and coneCTexpressIV 1.54 (Comscantecno). Samples were scanned at a magnification factor of 5.263 and spatial resolution of 19.001 μm/pixel. Captured images were rendered using the machine software TRI/3D BON (Ratoc System Engineering Co., Ltd., Tokyo, Japan).

Histological findings of bone tissues

Tibias were fixed with 4% paraformaldehyde in phosphate-buffered saline and decalcified with 10% ethylenediaminetetraacetic acid. Bone tissues were cut into thin sections (7μm) and stained with H&E (Wako, Osaka, Japan). Stained sections were observed with a light microscope (NIS element BR 3.0; Nikon, Tokyo, Japan).

Immunofluorescence staining

Bone tissues were cut into thin sections (7μm) and stained.

Immunofluorescence staining of TRACP and RANK were performed. Bone samples were incubated with primary and secondary antibodies (Supplementary Tables S1 and S2). Nuclei were stained with DAPI (Dojindo Laboratories, Kumamoto, Japan) and observed by confocal laser scanning microscopy (LSM 510; Carl Zeiss, Oberkochen, Germany).

Measurement of serum TRACP levels

Blood samples were obtained through cardiac puncture at sacrifice, and serum was separated and stored at -80 °C until use. Serum TRACP levels were measured with a Rat TRACP & ALP Assay Kit (Takara Bio, Inc., Shiga, Japan) according to the manufacturer's instructions.

Isolation, culture, and characterization of BM-MSCs

Bone marrow was collected from OVX and Sham rats. Bone marrow cells were harvested from OVX rats at 12 weeks after ovariectomy (OVX-MSCs) or Sham rats at 12 weeks after sham operation (Sham-MSCs). BM-MSCs were harvested by adherent cultures of bone marrow cells as described previously[49]. Characterization of rat BM-MSCs was performed by assessing their immunophenotype and differentiation potentials. The primary and secondary antibodies used for fluorescence-activated cell sorting are listed in Supplementary Tables S3 and S4.

Phase contrast microscopic observation of BM-MSCs

Morphological findings of BM-MSCs were observed by phase contrast microscopy (Eclipse TE200; Nikon, Tokyo, Japan).

Proliferation assays of BM-MSCs

Population doubling time (TD) was measured at P2 and calculated using the formula: TD = tplg2 / (lgNH − lgNI), where NI is the inoculum cell number, NH is the cell harvest number, and t is the time of the culture (in hours). The mean and standard deviation were calculated for three independent experiments. Statistical analysis was carried out using a t test. *P*-values < 0.05 were considered significant[50].

We plated 2.5×10^3 BM-MSCs at P2 in 96-well cell culture plates (Corning Costar; Sigma-Aldrich, St. Louis, MO, USA) and they were cultured for 24–72 h. Triplicate wells were used for each sample. Proliferation of BM-MSCs was analyzed using a Cell Counting Kit-8 (Dojindo Laboratories, Kumamoto, Japan). Briefly, the cells were treated with 10 μL WST-8 for another 2 h. Absorbance at 490 nm (A450) was measured with a microplate reader (Infinite M1000 Pro; TECAN, Männedorf, Switzerland).

Quantitative real-time reverse transcription-polymerase chain reaction (RT-PCR) of BM-MSCs

Total RNA was extracted using TRI Reagent (Molecular Research Center, Inc., Cincinnati, OH), and 1 μg total RNA was reverse-transcribed into cDNA with oligo-dT primers (Promega, Madison, WI) using the Omniscript RT kit (Qiagen, Hilden, Germany). Quantitative PCR was performed using ABI PRISM 7500 Real-Time PCR System (Applied Biosystems, Foster City, CA) with Universal SYBR PCR Master Mix (PerkinElmer, Covina, CA). Thermal cycling conditions were as follows: for 40 cycles of a two-step amplification (95°C for 15 seconds and 60°C for 1 minutes). Data were analyzed using comparative Ct Method (ΔΔCT Method). Specific primers used for rat *Runx2*, *Ocn*, *Erα* and *Opg* are shown in Supplementary Table S5. The rat *Gapdh* primer acted as an internal standard for RNA integrity and quantity. All PCRs were performed at least in duplicate.

Osteogenic differentiation of BM-MSCs

The multilineage differentiation potential of BM-MSCs was identified by culturing the cells. MSCs were plated at a concentration of 4.2 × 10^3 cells/cm^2 on a 4-well slide with MSC culture medium and incubated at 37 °C and 5% CO_2. When the cells were at 70% confluency 24–48 h later, the medium was changed with 500 µL osteogenic differentiation medium. The osteogenic differentiation medium was replaced every 3 days. After the BM-MSCs were cultured in osteogenic differentiation medium for 21 days, they were stained with ALP.

Adipogenic differentiation of BM-MSCs

The multilineage differentiation potential of BM-MSCs was identified by culturing the cells. BM-MSCs were plated at a concentration of 2.1 × 10^4 cells/cm^2 on a 4-well slide with MSC culture medium and incubated at 37 °C and 5% CO_2. When the cells were 100% confluent at 24–48 h later, the medium was changed with 500 µL adipogenic differentiation medium. The adipogenic differentiation medium was replaced every 3 days. After the BM-MSCs were cultured in adipogenic differentiation medium for 14 days, they were stained with Oil Red O.

Preparation of Wharton's jelly extract supernatant (WJS) from UC tissues

UC were washed with saline to remove blood components. Whole tissues of

UC were cut into short pieces in the longitudinal axis direction of amnion. All of the sectioned sheathes of amnion, UC vessels and Wharton's jelly were collected and wet weight was measured. Tissues were suspended in serum-free medium and shaken for 72 hours at 4°C. The supernatants of the tissue suspensions were obtained by centrifugation for 10 minutes at 300 ×g at 4°C. Supernatants, what we call WJS, were collected and quantified the protein concentrations with bicinchoninic acid (BCA) Protein Assay Kit (Thermo Fisher Scientific).

Activation of OVX-MSCs

WJS were added on OVX-MSCs at concentration 0.25 mg/ml. BM-MSCs was analyzed by cell morphology, proliferative potential, differentiation potential and mRNA expressions at 48 hours after administration of WJS.

Intravenous administration of BM-MSCs

At 4 weeks after ovariectomy, OVX rats were administered with vehicle or 1×10^4 Sham-MSCs (OVX-Sham-MSCs) or OVX-MSCs (OVX-OVX-MSCs) or OVX-MSCs activated with WJS (OVX-OVX-MSCs-WJ) /g body weight via the tail. Each BM-MSCs were administered with passage 3.

Regulation of osteoclast activity by BM-MSCs *in vitro*

Osteoclastogenesis of monocytes/macrophages was conducted by modifying the method of Yonezawa et al.[51]. We used the murine RAW264.7 monocyte/macrophage cell line (ATCC, Manassas, VA, USA) as osteoclast precursors. The cells were grown to subconfluence in a T75 standard flask with Dulbecco's modified Eagle's medium (DMEM) (Wako Pure Chemical, Osaka, Japan) supplemented with 10% heat-inactivated fetal bovine serum (FBS) (Invitrogen, Frederick, MD, USA) and 1% penicillin-streptomycin-glutamine 100× (1% PS) at 37 °C in a humidified atmosphere of 5% CO_2.

Subsequently, RAW264.7 cells were transferred to 12-well culture plates and cultured with DMEM supplemented with 15% heat-inactivated FBS and 1% PS at 37 °C in a humidified atmosphere of 95% air and 5% CO_2. After 24 h, the culture medium was changed to α-MEM (Wako Pure Chemical, Osaka, Japan) supplemented with 15% heat-inactivated FBS and 1% PS. For differentiation into mature osteoclasts, RAW264.7 cells (5.0×10^4 cells/well in 12-well culture plates) were cultured for 72 h in the presence of RANKL (100 ng/mL) and/or PD98059 (20 mM), a MAPK inhibitor that accelerates osteoclastogenesis. Cell morphology and supernatant TRACP levels were evaluated.

Co-culture of induced-osteoclasts and BM-MSCs

To investigate the functional effect of BM-MSCs on osteoclasts, RAW264.7 cells were cultured in the presence of RANKL or RNKL and PD98059. After 48 h, osteoclastic cells differentiated from RAW264.7 cells were indirectly co-cultured with P4 BM-MSCs (2.5×10^4 cells/cell culture insert 0.4 μm pore size). After 24 h co-culture, cell morphology, supernatant TRACP levels, and osteoclast-related genes were evaluated. The mRNA expression of osteoclast-related genes was determined with quantitative real-time RT-PCR. The primers used are listed in Supplementary Table S6.

Approval of the ethics committee

The human study was conducted in accordance with the ethical principles of the Declaration of Helsinki and was approved by the Ethics Committee of Sapporo Medical University (Registration numbers; 24-142, 25-1227, 262-1031, 262-1046, 262-110). Written informed consent was received from participants prior to their inclusion in the study.

Statistical analysis

Data from quantitative experiments were expressed as mean ± standard error (SE) values. Statistical significance was analyzed with the nonparametric Mann–Whitney test or Wilcoxon matched-pair test for group comparisons. Differences were considered significant at $P < 0.05$ in all two-tailed tests. Statistical analysis was performed using SPSS software (version 16.0; SPSS, Inc., Chicago, IL, USA).

References

1 Pacifici, R. Estrogen deficiency, T cells and bone loss. *Cellular immunology* **252**, 68-80 (2008).

2 Martin-Millan, M. *et al.* The estrogen receptor-alpha in osteoclasts mediates the protective effects of estrogens on cancellous but not cortical bone. *Mol Endocrinol* **24**, 323-334, doi:10.1210/me.2009-0354 (2010).

3 Raisz, L. G. Pathogenesis of osteoporosis: concepts, conflicts, and prospects. *J Clin Invest* **115**, 3318-3325, doi:10.1172/JCI27071 (2005).

4 Pittenger, M. F. & Martin, B. J. Mesenchymal stem cells and their potential as cardiac therapeutics. *Circ Res* **95**, 9-20, doi:10.1161/01.RES.0000135902.99383.6f (2004).

5 Kern, S., Eichler, H., Stoeve, J., Kluter, H. & Bieback, K. Comparative analysis of mesenchymal stem cells from bone marrow, umbilical cord blood, or adipose tissue. *Stem cells* **24**, 1294-1301, doi:10.1634/stemcells.2005-0342 (2006).

6 Chen, J. *et al.* Neuroprotective effect of human placenta-derived cell treatment of stroke in rats. *Cell Transplant* **22**, 871-879, doi:10.3727/096368911X637380 (2013).

7 Gronthos, S., Mankani, M., Brahim, J., Robey, P. G. & Shi, S. Postnatal human dental pulp stem cells (DPSCs) in vitro and in vivo. *Proceedings of the National Academy of Sciences of the United States of America* **97**, 13625-13630, doi:10.1073/pnas.240309797 (2000).

8 Bernardo, M. E. & Fibbe, W. E. Safety and efficacy of mesenchymal stromal cell therapy in autoimmune disorders. *Annals of the New York Academy of Sciences* **1266**, 107-117, doi:10.1111/j.1749-6632.2012.06667.x (2012).

9 Liang, J. *et al.* Allogenic mesenchymal stem cells transplantation in refractory systemic lupus erythematosus: a pilot clinical study. *Ann Rheum Dis* **69**, 1423-1429, doi:10.1136/ard.2009.123463 (2010).

10 Nagaishi, K., Ataka, K., Echizen, E., Arimura, Y., Fujimiya, M. . Mesenchymal stem cell therapy ameliorates diabetic hepatocyte damage in mice by inhibiting infiltration of bone marrow-derived cells. *Hepatology* **59**, 1816-1829, doi:10.1002/hep.26975 (2014).

11 Zilka, N. *et al.* Mesenchymal stem cells rescue the Alzheimer's disease cell model from cell death induced by misfolded truncated tau. *Neuroscience* **193**, 330-337, doi:10.1016/j.neuroscience.2011.06.088 (2011).

12 Nagaishi, K., Arimura, Y. & Fujimiya, M. Stem cell therapy for inflammatory bowel disease. *J Gastroenterol* **50**, 280-286, doi:10.1007/s00535-015-1040-9 (2015).

13 Jay G. Shake, M., Peter J. Gruber, MD, PhD, William A. Baumgartner, MD, Guylaine Senechal, MS, Jennifer Meyers, BS, J. Mark Redmond, MD, Mark F. Pittenger, PhD, and Bradley J. Martin, PhD. Mesenchymal Stem Cell Implantation in a Swine Myocardial Infarct Model: Engraftment and Functional Effect. *Ann Thorac Surg* **73**, 1919–1926 (2002).

14 Osaka, M. *et al.* Intravenous administration of mesenchymal stem cells derived from bone marrow after contusive spinal cord injury improves functional outcome. *Brain Res* **1343**, 226-235, doi:10.1016/j.brainres.2010.05.011 (2010).

15 Hsiao, F. S. *et al.* Isolation of therapeutically functional mouse bone marrow mesenchymal stem cells within 3 h by an effective single-step plastic-adherent method. *Cell Prolif* **43**, 235-248, doi:10.1111/j.1365-2184.2010.00674.x (2010).

16 Zhao, J. W., Gao, Z. L., Mei, H., Li, Y. L., Wang, Y. . Differentiation of Human Mesenchymal Stem Cells: The Potential Mechanism for Estrogen-Induced Preferential Osteoblast Versus Adipocyte Differentiation *The*

American journal of the medical sciences **341**, 460-468, doi: 10.1097/MAJ.0b013e31820865d5 (2011).

17 Bidwell, J. P., Alvarez, M. B., Hood, M., Jr. & Childress, P. Functional impairment of bone formation in the pathogenesis of osteoporosis: the bone marrow regenerative competence. *Curr Osteoporos Rep* **11**, 117-125, doi:10.1007/s11914-013-0139-2 (2013).

18 Chen, F.-P., Hu, C.-H. & Wang, K.-C. Estrogen modulates osteogenic activity and estrogen receptor mRNA in mesenchymal stem cells of women. *Climacteric* **16**, 154-160, doi:10.3109/13697137.2012.672496 (2012).

19 Turgeman, G. *et al.* Systemically administered rhBMP-2 promotes MSC activity and reverses bone and cartilage loss in osteopenic mice. *Journal of cellular biochemistry* **86**, 461-474 (2002).

20 Li, C. *et al.* Proliferation and Differentiation of Rat Osteoporosis Mesenchymal Stem Cells (MSCs) after Telomerase Reverse Transcriptase (TERT) Transfection. *Med Sci Monit* **21**, 845-854, doi:10.12659/MSM.893144 (2015).

21 Wang, Q. *et al.* Decreased proliferation ability and differentiation potential of mesenchymal stem cells of osteoporosis rat. *Asian Pacific Journal of Tropical Medicine* **7**, 358-363, doi:10.1016/s1995-7645(14)60055-9 (2014).

22 Majore, I., Moretti, P., Stahl, F., Hass, R. & Kasper, C. Growth and differentiation properties of mesenchymal stromal cell populations derived from whole human umbilical cord. *Stem cell reviews* **7**, 17-31, doi:10.1007/s12015-010-9165-y (2011).

23 Pa¯ka, J., Ba°kowski, E. & Jaworski, S. An accumulation of IGF-I and IGF-binding proteins in human umbilical cord. *Molecular and Cellular Biochemistry* **206**, 133-139 (2000).

24 Rao, C. V., Li, X., Toth, P. & Lei, Z. Expression of epidermal growth factor, transforming growth factor-alpha, and their common receptor genes in human umbilical cords. *The Journal of Clinical Endocrinology & Metabolism* **80**, 1012-1020 (1995).

25 An, J. H. *et al.* Transplantation of human umbilical cord blood-derived mesenchymal stem cells or their conditioned medium prevents bone loss in ovariectomized nude mice. *Tissue Eng Part A* **19**, 685-696, doi:10.1089/ten.TEA.2012.0047 (2013).

26 Hao, H. *et al.* Culturing on Wharton's jelly extract delays mesenchymal stem cell senescence through p53 and p16INK4a/pRb pathways. *PLoS One* **8**, e58314, doi:10.1371/journal.pone.0058314 (2013).

27 Igura, K., Okada, M., Kim, H. W. & Ashraf, M. Identification of small juvenile stem cells in aged bone marrow and their therapeutic potential for repair of the ischemic heart. *Am J Physiol Heart Circ Physiol* **305**, H1354-1362, doi:10.1152/ajpheart.00379.2013 (2013).

28 Wei, J. *et al.* Glucose Uptake and Runx2 Synergize to Orchestrate Osteoblast Differentiation and Bone Formation. *Cell* **161**, 1576-1591, doi:10.1016/j.cell.2015.05.029 (2015).

29 Chapurlat, R. D. & Confavreux, C. B. Novel biological markers of bone: from bone metabolism to bone physiology. *Rheumatology (Oxford)* **55**, 1714-1725, doi:10.1093/rheumatology/kev410 (2016).

30 Almeida, M. *et al.* Estrogen receptor-alpha signaling in osteoblast progenitors stimulates cortical bone accrual. *J Clin Invest* **123**, 394-404, doi:10.1172/JCI65910 (2013).

31 Kobayashi, Y., Udagawa, N. & Takahashi, N. Action of RANKL and OPG for osteoclastogenesis. *Crit Rev Eukaryot Gene Expr* **19**, 61-72 (2009).

32 Xiang, A. *et al.* Changes in micro-CT 3D bone parameters reflect effects of a potent cathepsin K inhibitor (SB-553484) on bone resorption and cortical bone

formation in ovariectomized mice. *Bone* **40**, 1231-1237, doi:10.1016/j.bone.2007.01.010 (2007).

33 Ulrich, C. *et al.* Low osteogenic differentiation potential of placenta-derived mesenchymal stromal cells correlates with low expression of the transcription factors Runx2 and Twist2. *Stem Cells Dev* **22**, 2859-2872, doi:10.1089/scd.2012.0693 (2013).

34 Lee, Y. S. *et al.* Twist2, a novel ADD1/SREBP1c interacting protein, represses the transcriptional activity of ADD1/SREBP1c. *Nucleic Acids Res* **31**, 7165-7174 (2003).

35 Sobolewski, K., Malkowski, A., Bankowski, E. & Jaworski, S. Wharton's jelly as a reservoir of peptide growth factors. *Placenta* **26**, 747-752, doi:10.1016/j.placenta.2004.10.008 (2005).

36 Franc, S., Rousseau, J. C., Garrone, R., Van der Rest, M., & Moradi-Ameli, M. . Microfibrillar composition of umbilical cord matrix: characterization of fibrillin, collagen VI and intact collagen V. *Placenta* **19**, 95-104 (1998).

37 Patel, A. N., Vargas, V., Revello, P. & Bull, D. A. Mesenchymal stem cell population isolated from the subepithelial layer of umbilical cord tissue. *Cell Transplant* **22**, 513-519, doi:10.3727/096368912X655064 (2013).

38 Khan, M., Akhtar, S., Mohsin, S., S, N. K. & Riazuddin, S. Growth factor preconditioning increases the function of diabetes-impaired mesenchymal stem cells. *Stem Cells Dev* **20**, 67-75, doi:10.1089/scd.2009.0397 (2011).

39 Eom, Y. W. *et al.* The role of growth factors in maintenance of stemness in bone marrow-derived mesenchymal stem cells. *Biochem Biophys Res Commun* **445**, 16-22, doi:10.1016/j.bbrc.2014.01.084 (2014).

40 Fekete, N. *et al.* Platelet lysate from whole blood-derived pooled platelet concentrates and apheresis-derived platelet concentrates for the isolation and expansion of human bone marrow mesenchymal stromal cells: production process, content and identification of active components. *Cytotherapy* **14**, 540-554, doi:10.3109/14653249.2012.655420 (2012).

41 Kerpedjieva, S. S., Kim, D. S., Barbeau, D. J. & Tamama, K. EGFR ligands drive multipotential stromal cells to produce multiple growth factors and cytokines via early growth response-1. *Stem Cells Dev* **21**, 2541-2551, doi:10.1089/scd.2011.0711 (2012).

42 Minayi, N. *et al.* The Effect of miR-210 Up-regulation on Proliferation and Survival of Mouse Bone Marrow Derived Mesenchymal Stem Cell. *Int J Hematol Oncol Stem Cell Res* **8**, 15-23 (2014).

43 Lv, C. *et al.* Role and mechanism of microRNA-21 in H2O2-induced apoptosis in bone marrow mesenchymal stem cells. *J Clin Neurosci* **27**, 154-160, doi:10.1016/j.jocn.2015.07.029 (2016).

44 Hong, I. S. & Kang, K. S. The effects of Hedgehog on the RNA-binding protein Msi1 in the proliferation and apoptosis of mesenchymal stem cells. *PLoS One* **8**, e56496, doi:10.1371/journal.pone.0056496 (2013).

45 Boyce, B. F. & Xing, L. Functions of RANKL/RANK/OPG in bone modeling and remodeling. *Arch Biochem Biophys* **473**, 139-146, doi:10.1016/j.abb.2008.03.018 (2008).

46 Pacifici, R. Estrogen, cytokines, and pathogenesis of postmenopausal osteoporosis. *J Bone Miner Res* **11**, 1043-1051, doi:10.1002/jbmr.5650110802 (1996).

47 Cutler, A. J., Limbani, V., Girdlestone, J. & Navarrete, C. V. Umbilical cord-derived mesenchymal stromal cells modulate monocyte function to suppress T cell proliferation. *J Immunol* **185**, 6617-6623, doi:10.4049/jimmunol.1002239 (2010).

48 Waynforth, H. B., & Flecknell, P. A. Experimental and surgical technique in the rat *Experimental and Surgical Technique in the RatSecond Edition* **127**, 161-163 (1980).

49 Javazon, E. H., Colter, D. C., Schwarz, E. J. & Prockop, D. J. Rat marrow stromal cells are more sensitive to plating density and expand more rapidly from single-cell-derived colonies than human marrow stromal cells. *Stem Cells* **19**, 219-225, doi:10.1634/stemcells.19-3-219 (2001).

50 Nekanti, U., Dastidar, S., Venugopal, P., Totey, S. & Ta, M. Increased Proliferation and Analysis of Differential Gene Expression in Human Wharton's Jelly-derived Mesenchymal Stromal Cells under Hypoxia. *International Journal of Biological Sciences* (2010).

51 Yonezawa, T. *et al.* Biselyngbyaside, isolated from marine cyanobacteria, inhibits osteoclastogenesis and induces apoptosis in mature osteoclasts. *J Cell Biochem* **113**, 440-448, doi:10.1002/jcb.23213 (2012).

Acknowledgements

The authors would like to thank Kozue Kamiya, Yuko Hayakawa, and Tatsuya Shiraishi, research assistants in the Second Department of Anatomy, for excellent technical support.

Author Contributions Statement

A.S. and K.N. designed the study, performed the experiments, analyzed the data, and wrote the paper. K.I., Y.M., T.C., M.O., and M.N. supported analyzing the data and reviewed the paper. T.Y. and M.F. coordinated the study and wrote the paper.

Additional Information

Competing financial interests

The authors have declared no competing financial interests.

Figure legends

Figure 1. Abnormalities of bone findings in OVX rat

(a) Experimental protocol for Sham and OVX rats. (b) Representative micro-CT images of tibias. (c–f) Quantitative changes in trabecular parameters, including trabecular bone volume expressed as c: BV/TV (percentage of total tissue volume), d: Tb.Th (trabecular thickness), e: Tb.N (trabecular number), and f: Tb.Sp (trabecular separation). $^{*}P < 0.05$. Data are expressed as mean ± SE of 4–5 animals. (g) Histological findings of the tibia in H&E-stained sections at 12 weeks after Sham and OVX operation in rats. Bar: upper 500 μm, lower 100 μm. (h) Immunofluorescence staining of the tibia with anti-RANK antibody (red). DAPI was used for counterstaining nuclei (blue). Bar: 25 μm. (i) Immunofluorescence staining of the tibia with anti-TRACP antibody (red). DAPI was used for counterstaining nuclei (blue). Bar: upper 50 μm, lower 25 μm. (j) Serum TRACP levels at 12 weeks after Sham and OVX operation in rats. $^{*}P < 0.05$. Data are expressed as mean ± SE of 4–5 animals.

Figure 2. Abnormalities of BM-MSCs derived from OVX rats

(a) Phase contrast observations of Sham-MSCs (left panel) and OVX-MSCs (right panel). The images were obtained from P0, P1, and P2 cells at 12 weeks after surgery.

Bar: 100 μm. (b) Immunophenotype expression of cell surface antigens analyzed by flow cytometry. Upper panels: Sham-MSCs; lower panels: OVX-MSCs. (c) Population doubling time of P2 Sham-MSCs vs. OVX-MSCs. *$P < 0.05$. Data are expressed as mean ± SE of 10 MSCs. (d) MTT assay of P3 Sham-MSCs vs. OVX-MSCs. *$P < 0.05$. Data are expressed as mean ± SE of 5 MSCs. (e-g) Relative expressions of mRNA in BM-MSCs. Values are means ± SE of the Sham-MSCs (n=4) and OVX-MSCs (n=3). * $P < 0.05$. Data are expressed as mean ± SE of 3–5 animals. *Runx2*, Runt-related transcription factor 2; *Ocn*, osteocalcin; *Erα*, estrogen receptor α; *Opg*, osteoprotegerin. (h) Osteogenic and adipogenic differentiation of Sham-MSCs (left panel) and OVX-MSCs (right panel). The images were obtained at 14 days after culture with osteogenic or adipogenic differentiation medium. Bone matrixes are stained blue by ALP staining kit. Fat droplets are stained red with Oil red O staining. Bar: 100 μm.

Figure 3. Therapeutic effect of Sham-MSCs and OVX-MSCs in OVX rats

(a) Experimental protocol for Vehicle, Sham-MSCs, and OVX-MSCs therapies in OVX rats. (b) Representative micro-CT images of tibias. (c–f) Quantitative changes in trabecular parameters, including trabecular bone volume expressed as c: BV/TV (percentage of total tissue volume), d: Tb.Th (trabecular thickness), e: Tb.N (trabecular number), and f: Tb.Sp (trabecular separation). *$P < 0.05$. Data are expressed as mean ± SE of 4–5 animals. (g) Histological findings of the tibia in H&E-stained sections at 8 weeks after vehicle, Sham-MSCs, and OVX-MSCs therapies in OVX rats. Bar: 500 μm in upper panel, 100 μm in lower panel. (h) Immunofluorescence staining of the tibia with anti-RANK antibody (red). DAPI was used for counterstaining nuclei (blue). Bar: 25 μm. (i) Immunofluorescence staining of the tibia with anti-TRACP antibody (red). DAPI was used for counterstaining nuclei (blue). Bar: upper 50 μm, lower 25 μm. (j) Serum TRACP levels at 12 weeks after Sham and OVX operation in rats. *$P < 0.05$. Data are expressed as mean ± SE of 4–5 animals.

Figure 4. Activating effects of WJS for OVX-MSCs

(a) Phase contrast observations of OVX-MSCs without WJS (left panel) and OVX-MSCs activated with WJS (right panel). The images were obtained at 48 h after activation with WJS. Bar: 100 μm. (b) Immunophenotype expression of cell surface antigens analyzed by flow cytometry. Upper panels: OVX-MSCs-WJ(-); lower panels: OVX-MSCs-WJ(+). (c) Population doubling time of P4 OVX-MSCs-WJ(-) vs. OVX-

MSCs-WJ(+). *P < 0.05. Data are expressed as mean ± SE of 5 MSCs. (d) MTT assay of P4 OVX-MSCs-WJ(-) vs. OVX-MSCs-WJ(+). *P < 0.05. Data are expressed as mean ± SE of 5 MSCs. (e-g) Relative expressions of mRNA in BM-MSCs. Values are means ± SE of the OVX-MSCs-WJ(-) (n=3) and OVX-MSCs-WJ(+) (n=3). * P < 0.05. *Runx2*, Runt-related transcription factor 2; *Ocn*, osteocalcin; *Erα*, estrogen receptor α; *Opg*, osteoprotegerin. (h) Osteogenic and adipogenic differentiation of OVX-MSCs-WJ(-) (left panel) and OVX-MSCs-WJ(+) (right panel). The images were obtained at 14 days after culture with osteogenic or adipogenic differentiation medium. Bone matrixes are stained blue by ALP staining kit. Fat droplets are stained red with Oil red O staining. Bar: 100 μm.

Figure 5. Therapeutic effect of OVX-MSCs which are activated with WJS in OVX rats

(a) Experimental protocol for Vehicle, OVX-MSCs-WJ(-), and OVX-MSCs-WJ(+) therapies in OVX rats. (b) Representative micro-CT images of tibias. (c–f) Quantitative changes in trabecular parameters, including trabecular bone volume expressed as c: BV/TV (percentage of total tissue volume), d: Tb.Th (trabecular thickness), e: Tb.N (trabecular number), and f: Tb.Sp (trabecular separation). *P <

0.05. Data are expressed as mean ± SE of 4–5 animals. (g) Histological findings of the tibia in H&E-stained sections at 8 weeks after Vehicle, OVX-MSCs-WJ(-), and OVX-MSCs-WJ(+) therapies in OVX rats. Bar: 500 μm in upper panel, 100 μm in lower panel. (h) Immunofluorescence staining of the tibia with anti-RANK antibody (red). DAPI was used for counterstaining nuclei (blue). Bar: 25 μm. (i) Immunofluorescence staining of the tibia with anti-TRACP antibody (red). DAPI was used for counterstaining nuclei (blue). Bar: upper 50 μm, lower 25 μm. (j) Serum TRACP levels at 12 weeks after Sham and OVX operation in rats. $*P < 0.05$. Data are expressed as mean ± SE of 4–5 animals.

Figure 6. Osteoclast regulating ability of OVX-MSCs which are activated with WJS

(a) Experimental protocol to induce macrophage-derived osteoclasts using RAW264.7 cells. (b) Phase contrast observations of RAW264.7 cells cultured without RANKL (left panel), with RANKL (middle panel), and with RANKL and PD98059 (right panel). The images were obtained at 72 h after adding RANKL or RANKL and PD98059 to the culture medium. Bar: 500 μm in upper panel, 100 μm in lower panel. (c) TRACP levels in the supernatant of RAW264.7 cell-derived osteoclasts. $*P < 0.05$.

Data are expressed as mean ± SE of 3 experiment. (d) Experimental protocol for co-culture of RAW264.7 cell-derived osteoclasts with Vehicle, Sham-MSCs, OVX-MSCs-WJ(-), and OVX-MSCs-WJ(+). (e) Phase contrast observations of matured osteoclasts co-cultured without MSCs (left panel), and with Sham-MSCs (middle left panel), OVX-MSCs-WJ(-) (middle right panel), and OVX-MSCs-WJ(+) (right panel) using a transwell. The images were obtained at 72 h after adding RANKL and PD98059 to the culture medium and at 24 h after starting co-culture. Bar: 500 μm in upper panel, 100 μm in lower panel. (f) TRACP levels in the supernatant of RAW264.7 cell-derived osteoclasts co-cultured without MSCs and with Sham-MSCs, OVX-MSCs-WJ(-), and OVX-MSCs-WJ(+). Data are expressed as mean ± SE of osteoclasts. *$P < 0.05$. Data are expressed as mean ± SE of 3 experiments. (g) Relative expressions of mRNA in RAW264.7 cell-derived osteoclasts. Values are means ± SE of osteoclasts co-cultured without MSCs and with Sham-MSCs, OVX-MSCs-WJ(-), and OVX-MSCs-WJ(+). * $P < 0.05$. Data are expressed as mean ± SE of 3 experiments. *C-fms*, colony stimulating factor 1 receptor; *Nfatc1*, nuclear factor of activated T cells; *Cath-k*, cathepsin K; *Clc7*, chloride channel-7; *Atp6i*, ATPase, H^+ transporting, (vacuolar proton pump) member I; *Dc-stamp*, dendritic cell specific transmembrane protein.

Figure 7. Presumed activation mechanisms of WJS on OVX-MSCs and their therapeutic effects for osteoporosis

The site of action of WJS on OVX-MSCs and their therapeutic mechanism for osteoporosis.

Figure1

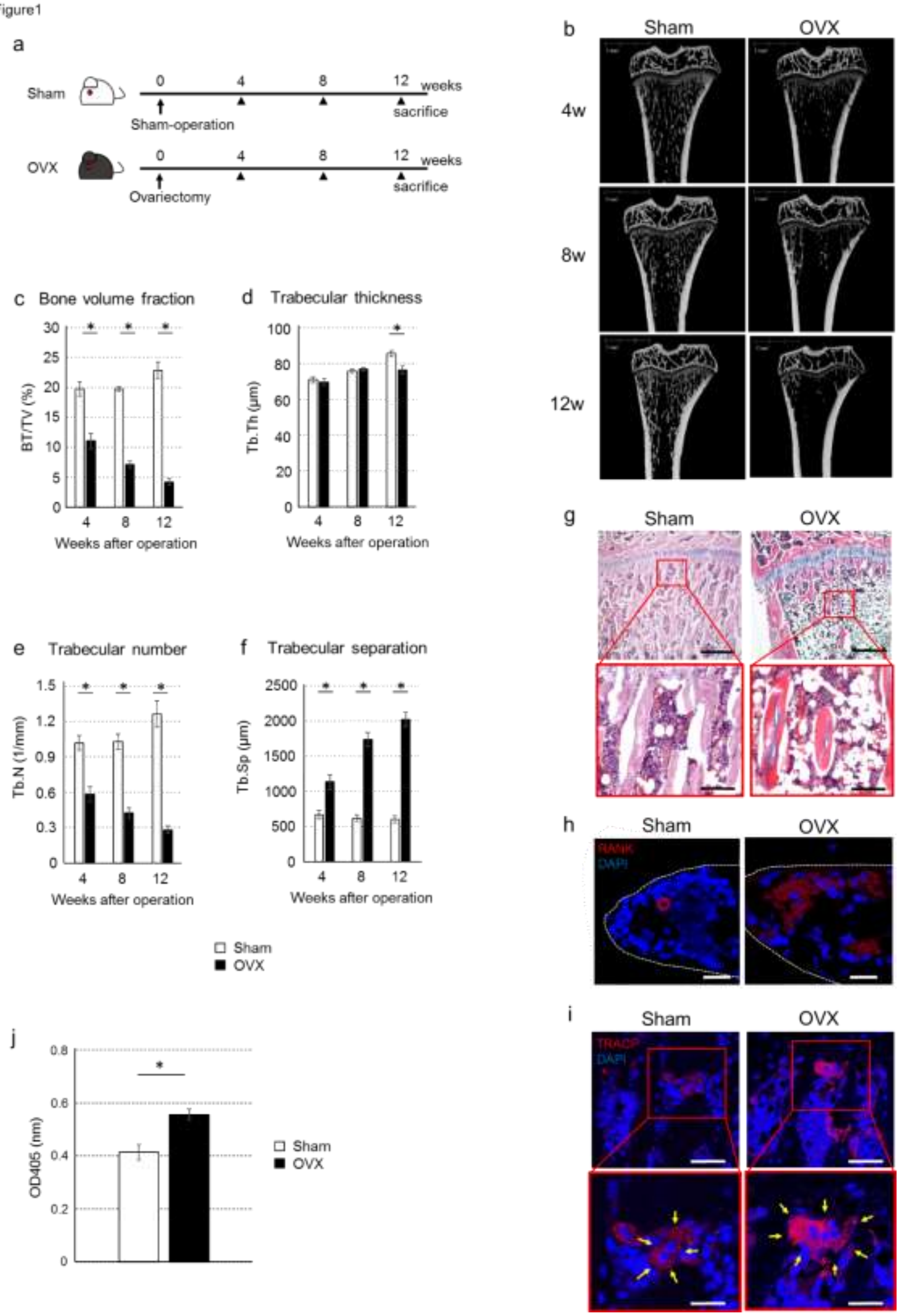
a
Sham
0
4
8
12
weeks
Sham-operation
sacrifice
OVX
Ovariectomy
c Bone volume fraction
BT/TV (%)
Weeks after operation
d Trabecular thickness
Tb.Th (µm)
e Trabecular number
Tb.N (1/mm)
f Trabecular separation
Tb.Sp (µm)
Sham
OVX
j
OD405 (nm)
b
4w
8w
12w
g
h
RANK
DAPI
i
TRACP

Figure2

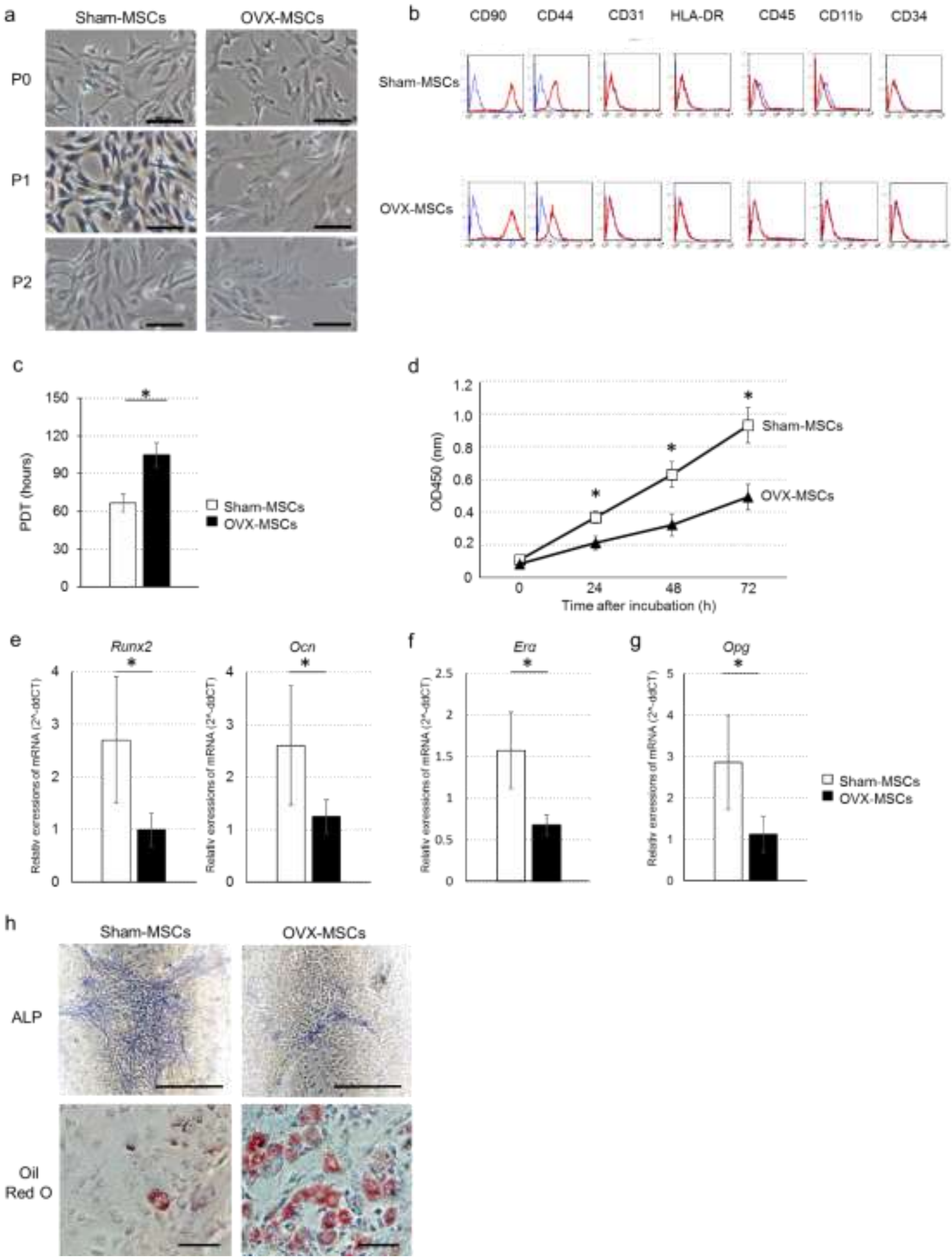
a
Sham-MSCs
OVX-MSCs
P0
P1
P2
b
CD90
CD44
CD31
HLA-DR
CD45
CD11b
CD34
Sham-MSCs
OVX-MSCs
c
PDT (hours)
Sham-MSCs
OVX-MSCs
d
OD450 (nm)
Time after incubation (h)
Sham-MSCs
OVX-MSCs
e
Runx2
Ocn
Relativ expressions of mRNA (2^-ddCT)
f
Erα
g
Opg
Sham-MSCs
OVX-MSCs
h
Sham-MSCs
OVX-MSCs
ALP
Oil
Red O

Figure3

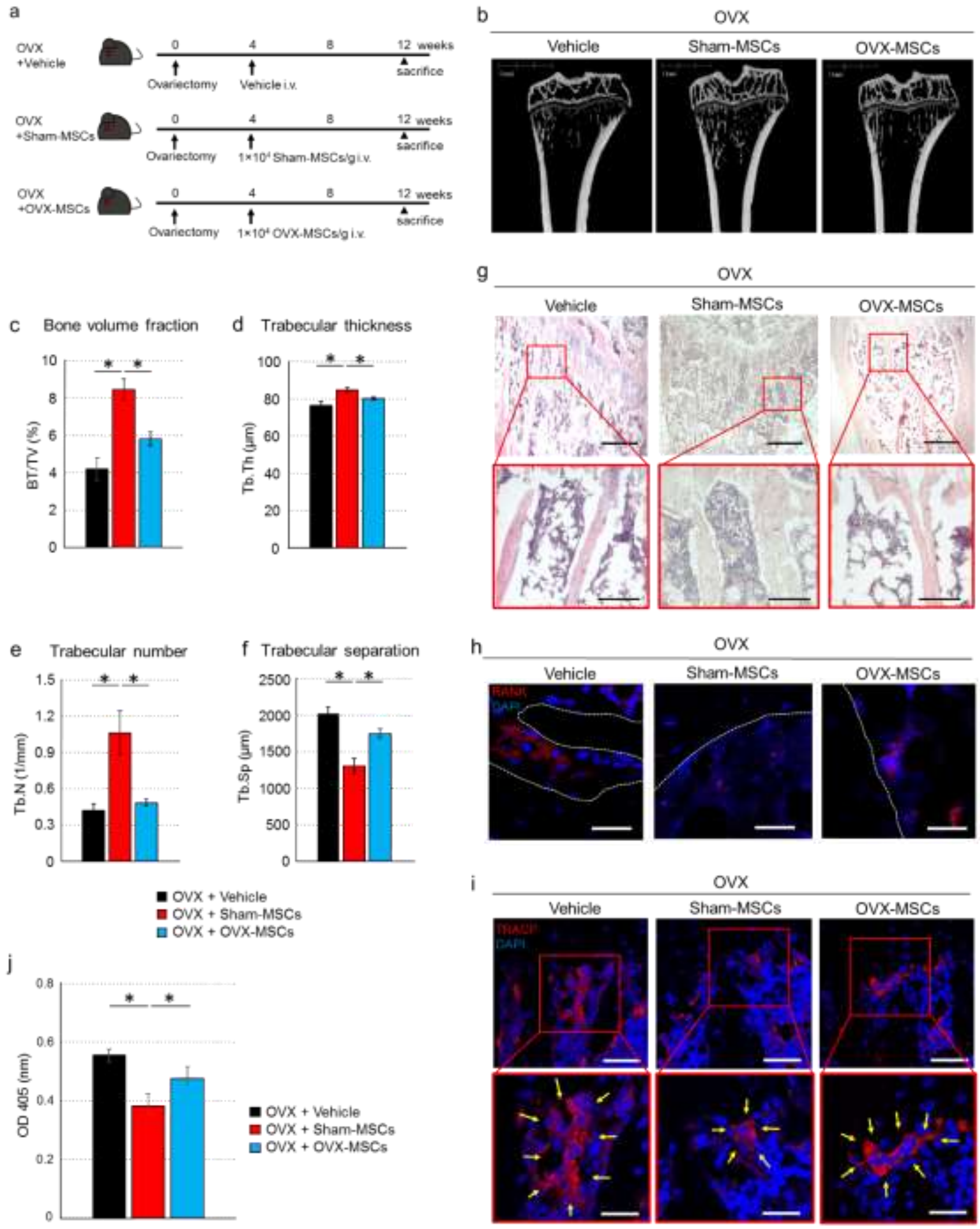
a
OVX +Vehicle
0 4 8 12 weeks
Ovariectomy
Vehicle i.v.
sacrifice
OVX +Sham-MSCs
Ovariectomy
1×10⁴ Sham-MSCs/g i.v.
OVX +OVX-MSCs
Ovariectomy
1×10⁴ OVX-MSCs/g i.v.
b
OVX
Vehicle
Sham-MSCs
OVX-MSCs
c Bone volume fraction
BT/TV (%)
d Trabecular thickness
Tb.Th (μm)
e Trabecular number
Tb.N (1/mm)
f Trabecular separation
Tb.Sp (μm)
OVX + Vehicle
OVX + Sham-MSCs
OVX + OVX-MSCs
g
h
RANK
DAPI
i
TRAP
DAPI
j
OD 405 (nm)

Figure4

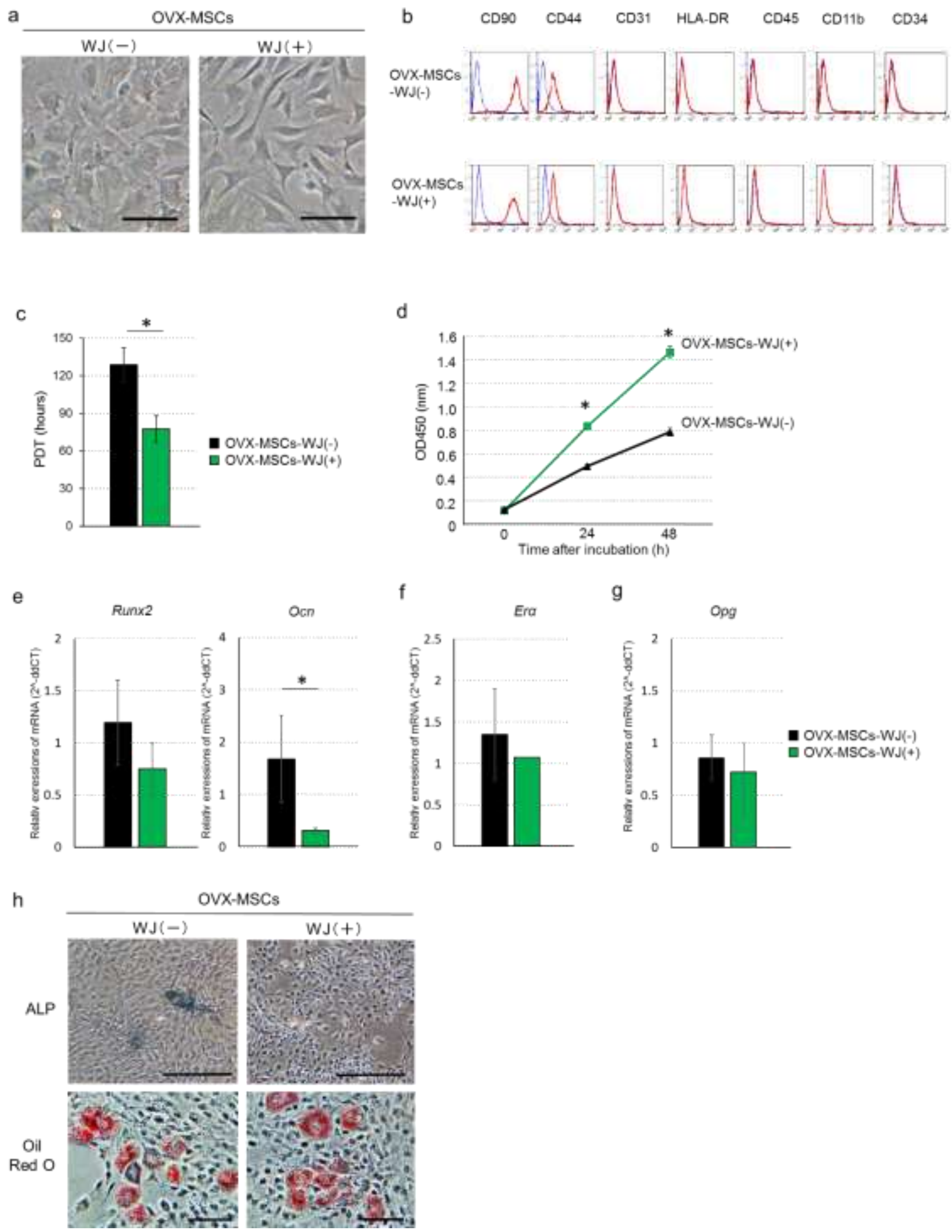
a
OVX-MSCs
WJ(−)
WJ(+)
b
CD90
CD44
CD31
HLA-DR
CD45
CD11b
CD34
OVX-MSCs -WJ(-)
OVX-MSCs -WJ(+)
c
PDT (hours)
150
120
90
60
30
0
*
OVX-MSCs-WJ(-)
OVX-MSCs-WJ(+)
d
OD450 (nm)
1.6
1.4
1.2
1.0
0.8
0.6
0.4
0.2
0
0
24
48
Time after incubation (h)
*
*
OVX-MSCs-WJ(+)
OVX-MSCs-WJ(-)
e
Runx2
Ocn
Relativ exressions of mRNA (2^-ddCT)
*
f
Erα
g
Opg
OVX-MSCs-WJ(-)
OVX-MSCs-WJ(+)
h
OVX-MSCs
WJ(−)
WJ(+)
ALP
Oil Red O

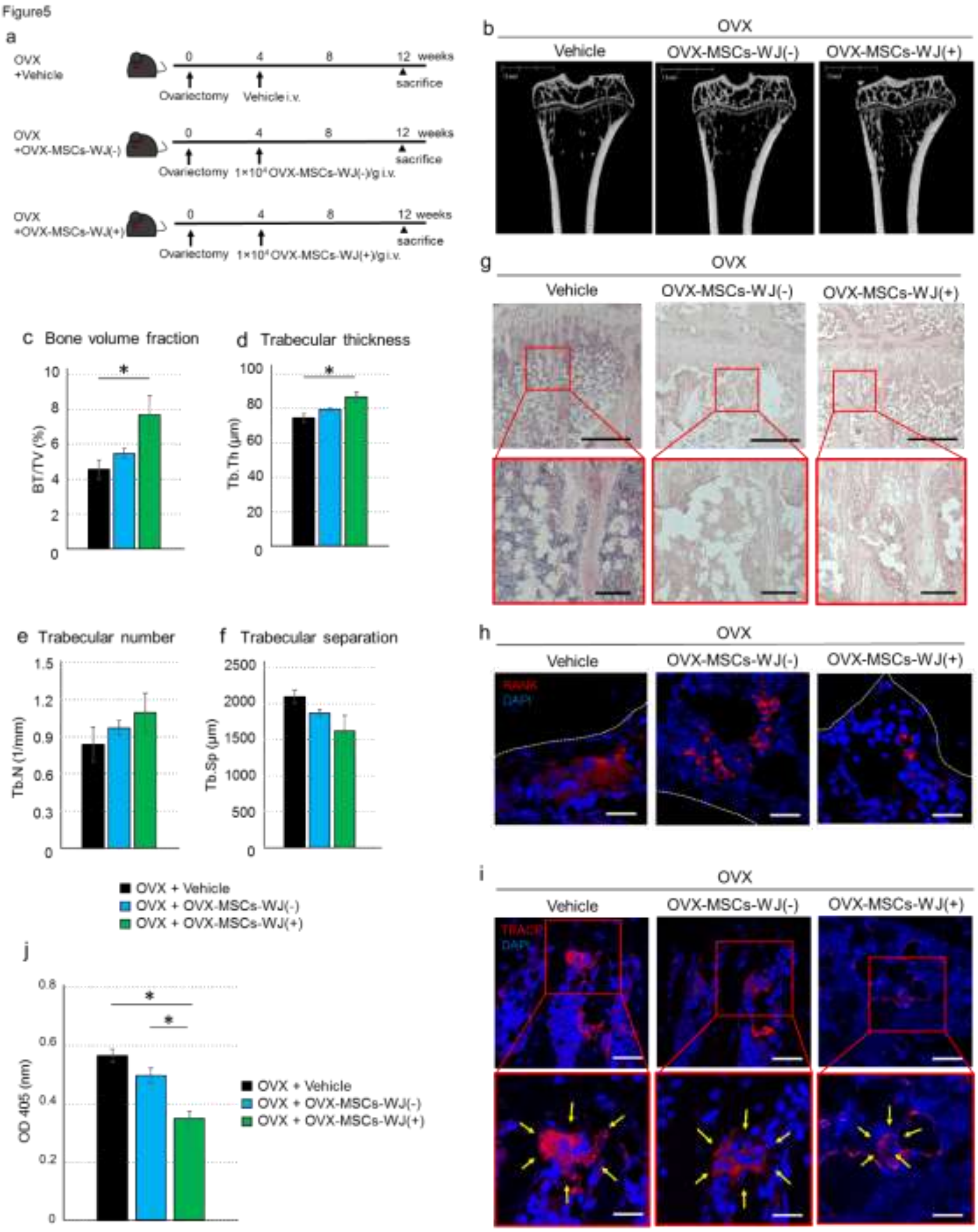
Figure5
a
OVX +Vehicle
0 4 8 12 weeks
Ovariectomy
Vehicle i.v.
sacrifice
OVX +OVX-MSCs-WJ(-)
1×10⁴ OVX-MSCs-WJ(-)/g i.v.
OVX +OVX-MSCs-WJ(+)
1×10⁴ OVX-MSCs-WJ(+)/g i.v.
b
OVX
Vehicle
OVX-MSCs-WJ(-)
OVX-MSCs-WJ(+)
c Bone volume fraction
BT/TV (%)
d Trabecular thickness
Tb.Th (µm)
e Trabecular number
Tb.N (1/mm)
f Trabecular separation
Tb.Sp (µm)
OVX + Vehicle
OVX + OVX-MSCs-WJ(-)
OVX + OVX-MSCs-WJ(+)
g
h
i
j
OD 405 (nm)

Figure6

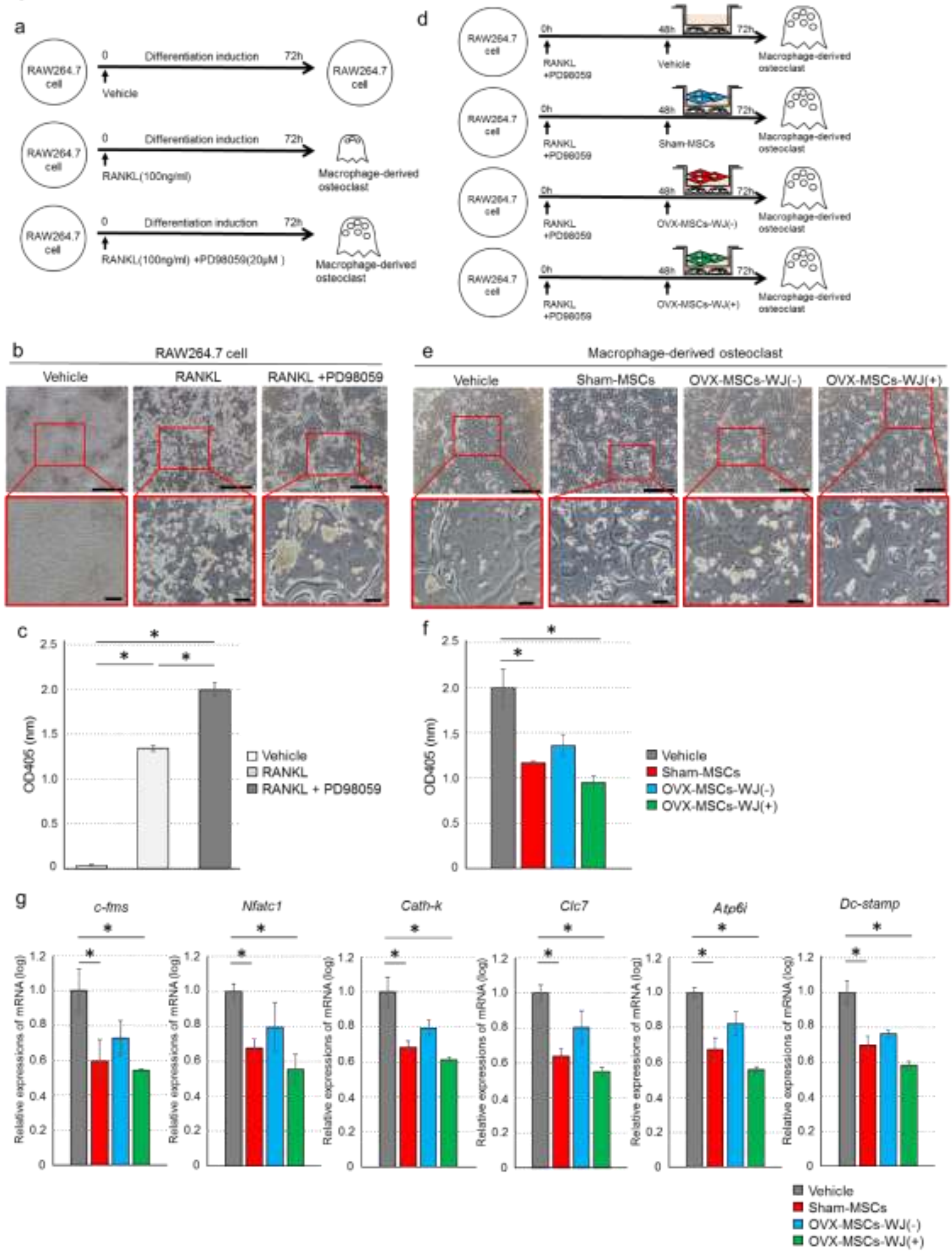
a
RAW264.7 cell
0
Differentiation induction
72h
Vehicle
RANKL(100ng/ml)
Macrophage-derived osteoclast
RANKL(100ng/ml) +PD98059(20μM)
d
0h
48h
72h
RANKL +PD98059
Vehicle
Sham-MSCs
OVX-MSCs-WJ(-)
OVX-MSCs-WJ(+)
b
RAW264.7 cell
Vehicle
RANKL
RANKL +PD98059
e
Macrophage-derived osteoclast
Vehicle
Sham-MSCs
OVX-MSCs-WJ(-)
OVX-MSCs-WJ(+)
c
OD405 (nm)
Vehicle
RANKL
RANKL + PD98059
f
OD405 (nm)
Vehicle
Sham-MSCs
OVX-MSCs-WJ(-)
OVX-MSCs-WJ(+)
g
c-fms
Nfatc1
Cath-k
Clc7
Atp6i
Dc-stamp
Relative expressions of mRNA (log)
Vehicle
Sham-MSCs
OVX-MSCs-WJ(-)
OVX-MSCs-WJ(+)

Figure 7

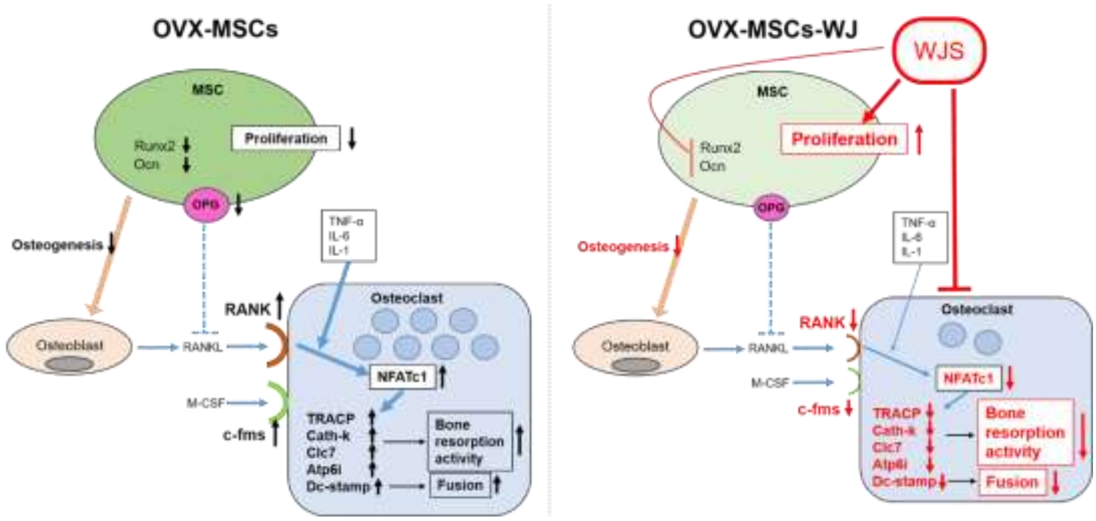

OVX-MSCs
MSC
Runx2
Ocn
Proliferation
OPG
Osteogenesis
TNF-α
IL-6
IL-1
Osteoclast
RANK
Osteoblast
RANKL
NFATc1
M-CSF
c-fms
TRACP
Cath-k
Clc7
Atp6i
Dc-stamp
Bone resorption activity
Fusion
OVX-MSCs-WJ
WJS
MSC
Runx2
Ocn
Proliferation
OPG
Osteogenesis
TNF-α
IL-6
IL-1
Osteoclast
RANK
Osteoblast
RANKL
NFATc1
M-CSF
c-fms
TRACP
Cath-k
Clc7
Atp6i
Dc-stamp
Bone resorption activity
Fusion

1
2

SUPPLEMENTARY INFORMATION

Title

Umbilical cord extracts improve osteoporosis-induced abnormalities of bone marrow-derived mesenchymal stem cells and promote their therapeutic effects on ovariectomized rats

Akira Saito, Kanna Nagaishi*, Kousuke Iba, Yuka Mizue, Takako Chikenji, Miho Otani, Masako Nakano, Toshihiko Yamashita, and Mineko Fujimiya

*Corresponding author

Supplementary Result

Distribution of Sham-MSCs in OVX rats

PKH26-labeled Sham-MSCs were distributed in the bone marrow of OVX rats at 24 h after cell administration. The number of distributed cells was decreased at day 3 and disappeared by 7 days after cell administration (Supplementary Fig. S1).

Supplementary Methods

Isolation, culture, and characterization of BM-MSCs

Bone marrow was collected from Sham rats and OVX rats. BM-MSCs were harvested by adherent cultures of bone marrow cells as described previously[1]. Briefly, bone marrow cells were harvested from femurs and tibias by flushing whole bone marrow with complete α-modified Eagle's medium (α-MEM; GIBCO BRL, Palo Alto, CA, USA) containing 15% fetal bovine serum and 1% penicillin-streptomycin. Bone marrow cells were suspended as single cells and plated. The cells were grown in complete α-MEM at 37°C and 5% CO_2. Adherent cells grown to confluency were defined as passage 0 (P0). Cells in P2-4 were used for experiments. Surface antigens of BM-MSCs were detected by fluorescence-activated cell sorting (Calibur; BD Bioscience, Franklin Lakes, NJ, USA) using rat surface antigen specific antibodies, CD90, CD44, CD31, HLA-DR, CD45, CD11b and CD34. The primary and secondary antibodies used for fluorescence-activated cell sorting are listed in Supplementary Tables S3 and S4. The *in vitro* differentiation potential of BM-MSCs was confirmed by previously described methods[2]. Briefly, BM-MSCs were cultured with adipogenic and osteogenic differentiation medium (TAKARA Bio, Inc. Kusatsu, Japan) for 3 weeks, following the manufacturer's instructions. Adipogenic differentiation was detected by Oil red O staining (Sigma-Aldrich, St. Louis, MO, USA). Osteogenic differentiation was detected using an Alkaline Phosphatase Staining Kit (Cosmo Bio Co., Ltd. Tokyo, Japan).

Detection of donor BM-MSCs

Sham-MSCs were labeled with a PKH26 Red Fluorescent Cell Linker Kits (Sigma-Aldrich) and administered to OVX rats by tail vein injection at 4 weeks after OVX. The rats were euthanized at 1, 3, or 7 days after BM-MSCs injection, and tibia were collected. The bones were immersed in 4% paraformaldehyde for 2 days, and decalcified with 0.5 M of ethylenediaminetetraacetic acid (Wako, Osaka, Japan) for 30 days. Frozen sections of each organ were stained with DAPI (Dojindo Laboratories, Kumamoto, Japan) at 0.1 mg/mL. The distribution of BM-MSCs expressing red fluorescence in bone was observed by confocal laser scanning microscopy (LSM 510;

Carl Zeiss, Oberkochen, Germany).

Supplementary References

1 Javazon, E. H., Colter, D. C., Schwarz, E. J. & Prockop, D. J. Rat marrow stromal cells are more sensitive to plating density and expand more rapidly from single-cell-derived colonies than human marrow stromal cells. *Stem Cells* **19**, 219-225, doi:10.1634/stemcells.19-3-219 (2001).

2 Romanov, Y. A., Svintsitskaya, V. A. & Smirnov, V. N. Searching for alternative sources of postnatal human mesenchymal stem cells: candidate MSC-like cells from umbilical cord. *Stem Cells* **21**, 105-110, doi:10.1634/stemcells.21-1-105 (2003).

Supplementary Figure Legends

Supplementary Figure S1. Distribution of Sham-MSCs in OVX rats

Distribution of administered Shma-MSCs in OVX rats at days 1, 3, and 7. Sham-MSCs were detected in bone with the immunofluorescence marker PKH26 (red) in bone. DAPI was used for counterstaining of nuclei (blue). The white arrows show the distribution of Sham-MSCs. White dotted line: trabeculae bone. Bar: 50 µm.

Supplementary Table Legends and Caption

Supplementary Table S1. Primary antibodies used for immunofluorescence

RANK, receptor activator of NF-κB, TRACP, tartrate-resistant acid phosphatase; Ms, mouse ; Rt, rat ; Hu, human.

Supplementary Table S2. Secondary antibodies used for immunofluorescence

Dnk, donkey.

Supplementary Table S3. Primary antibodies used for fluorescence-activated cell sorting analysis

Ms, mouse; Rt, rat; Hu, human.

Supplementary Table S4. Secondary antibodies used for fluorescence-activated cell sorting analysis

Dnk, donkey.

Supplementary Table S5. Primer sequences used for quantitative RT-PCR of rat BM-MSCs

Runx2, runt-related transcription factor 2; *Ocn*, osteocalcin; *Erα*, estrogen receptor α ; *Opg*, osteoprotegerin ; *Gapdh*, Glyceraldehyde 3-phosphate dehydrogenase

Supplementary Table S6. Primer sequences used for quantitative RT-PCR of RAW264.7 cells

C-fms, colonystimulating factor 1 receptor; *Nfatc1*, nuclear factor of activated T cells ; *Cath-k*, cathepsin K ; *Clc7*, chloride channel 7; *Atp6i*, ATPase, H^+ transporting, (vadcuolar proton pump) member I ; *Dc-stamp*, dendritic cell specific transmembrane protein ; *Gapdh*, **glyceraldehyde 3-phosphate dehydrogenase.**

Supplementary Tables

Supplementary Table S1. Primary antibodies used for immunofluorescence

Antibody	Species	Reactivity	Manufacturer
Immunofluorescence			
RANK	Rt	Ms, Rt, Hu	Santa Cruz Biotechnology
TRACP	Ms	Ms, Rt, Hu	BioLegend

Supplementary Table S2. Secondary antibodies used for immunofluorescence

Antibody	Species	Conjugate	Manufacturer
Immunofluorescence			
Anti-mouse IgG	Dnk	Cy3	Chemicon

Anti-rabbit igG	Dnk	Cy3	Jackson Laboratory

Supplementary Table S3. Primary antibodies used for fluorescence-activated cell sorting analysis

Antibody	Species	Reactivity	Manufacture
Immunophenotype			
CD90(Thy1.1)	Ms-IgG1	Ms, Rt	BioLegend
CD44	Ms-IgG1	Rt	BioLegend
CD31	Ms-IgG1	Rt	AbD Serotec
HLA-DR	Ms-IgG1	Rt	BioLegend
CD45	Ms-IgG2a	Rt	BioLegend
CD11b	Ms-IgG2a	Rt	BioLegend
CD34	Rb	Ms, Rt, Hu	BioLegend
Mouse IgG1		-	BD Bioscience
Mouse IgG2a		-	BD Bioscience
Rabbit IgG		-	BioLegend

Supplementary Table S4. Secondary antibodies used for fluorescence-activated cell sorting analysis

Antibody	Species	Conjugate	Manufacture
Immunophenotype			
Anti-mouse IgG	Dnk	FITC	Chemicon
Anti-rabbit IgG	Dnk	FITC	Chemicon

Supplementary Table S5. Primer sequences used for quantitative PCR of BM-MSCs

Gene	Locus	Direction	Sequence
Runx2	NM_001278483	forward	5’- *cagttcctaacgggcaccat* -3’
		reverse	5’- *ttagggtctcggagggaagg* -3’
Ocn	NM_013059	forward	5’- *gagcaggaacagaagtttgc* -3’
		reverse	5’- *gttgcagggtctggagagta* -3’
Erα	NM_012689	forward	5’- *aggagactcgctactgtgctg* -3’
		reverse	5’-atcatgcccacttcgtaacac -3’
Opg	NM_012870	forward	5’- *gccaacactgatggagcagat* -3’
		reverse	5’- *tcttcattcccaccaactgatg* -3’

Gapdh	NM_017008	forward	5’- *caaggatactgagagcaagaga* -3’
		reverse	5’- *aggcccctcctgttgttat* -3’

Supplementary Table S6. Primer sequences used for quantitative RT-PCR of RAW264.7 cells

Gene	Locus	Direction	Sequence
C-fms	NM_001029901	forward	5’- tgtcatcgagcctagtggc -3’
		reverse	5’- ggtccaaggtccagtaggg-3’
Nfatc1	NM_ 1164111	forward	5’- *cagtgtgaccgaagatacctgg*-3’
		reverse	5’- *tcgagacttgatagggaccccc*-3’
Cath-k	NM_007802	forward	5’- aatacctccctctcgatcctaca-3’
		reverse	5’- tggttcttgactggagtaacgta-3’
Clc7	NM_011930	forward	5’- gacaacagcgagaatcagctc-3’
		reverse	5’- ccaatgagggcacagataacc-3’
Atp6i	NM_ 001167784.	forward	5’- *attgccagctttcgggagac*-3’
		reverse	5’- *cggatcttctgtccgatctgc*-3’
Dc-stamp	NM_001289506	forward	5’- ctgtgtcctcccgctgaataa-3’
		reverse	5’- agccgatacagcagatagtcc-3’

Supplementary Figure S1

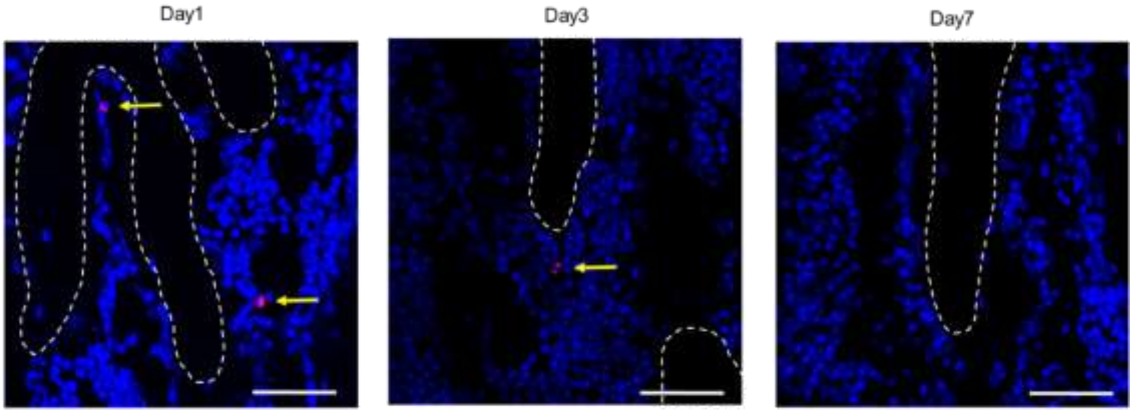

Gapdh	NM_01289726	forward	5’- tggccttccgtgttcctac-3’
		reverse	5’- gagttgctgttgaagtcgca-3’